arXiv:1110.3568v1 [hep-ph] 17 Oct 2011

Supersymmetry in Light of 1/fb of LHC Data

O. Buchmueller[a], **R. Cavanaugh**[b,c], **A. De Roeck**[d,e], **M.J. Dolan**[f], **J.R. Ellis**[g,d], **H. Flächer**[h], **S. Heinemeyer**[i], **G. Isidori**[j], **D. Martínez Santos**[d], **K.A. Olive**[k], **S. Rogerson**[a], **F.J. Ronga**[l], **G. Weiglein**[m]

[a]High Energy Physics Group, Blackett Laboratory, Imperial College, Prince Consort Road, London SW7 2AZ, UK

[b]Fermi National Accelerator Laboratory, P.O. Box 500, Batavia, Illinois 60510, USA

[c]Physics Department, University of Illinois at Chicago, Chicago, Illinois 60607-7059, USA

[d]CERN, CH–1211 Genève 23, Switzerland

[e]Antwerp University, B–2610 Wilrijk, Belgium

[f]Institute for Particle Physics Phenomenology, University of Durham, South Road, Durham DH1 3LE, UK

[g]Theoretical Particle Physics and Cosmology Group, Department of Physics, King's College London, London WC2R 2LS, UK

[h]H.H. Wills Physics Laboratory, University of Bristol, Tyndall Avenue, Bristol BS8 1TL, UK

[i]Instituto de Física de Cantabria (CSIC-UC), E–39005 Santander, Spain

[j]INFN, Laboratori Nazionali di Frascati, Via E. Fermi 40, I–00044 Frascati, Italy

[k]William I. Fine Theoretical Physics Institute, School of Physics and Astronomy, University of Minnesota, Minneapolis, Minnesota 55455, USA

[l]Institute for Particle Physics, ETH Zürich, CH–8093 Zürich, Switzerland

[m]DESY, Notkestrasse 85, D–22607 Hamburg, Germany

We update previous frequentist analyses of the CMSSM and NUHM1 parameter spaces to include the public results of searches for supersymmetric signals using $\sim$ 1/fb of LHC data recorded by ATLAS and CMS and $\sim$ 0.3/fb of data recorded by LHCb in addition to electroweak precision and B-physics observables. We also include the constraints imposed by the cosmological dark matter density and the XENON100 search for spin-independent dark matter scattering. The LHC data set includes ATLAS and CMS searches for jets $+\not{E}_T$ events and for the heavier MSSM Higgs bosons, and the upper limits on BR($B_s \to \mu^+\mu^-$) from LHCb and CMS. The absences of jets $+\not{E}_T$ signals in the LHC data favour heavier mass spectra than in our previous analyses of the CMSSM and NUHM1, which may be reconciled with $(g-2)_\mu$ if $\tan\beta \sim 40$, a possibility that is however under pressure from heavy Higgs searches and the upper limits on BR($B_s \to \mu^+\mu^-$). As a result, the p-value for the CMSSM fit is reduced to $\sim$ 15(38)%, and that for the NUHM1 to $\sim$ 16(38)%, to be compared with $\sim$ 9(49)% for the Standard Model limit of the CMSSM for the same set of observables (dropping $(g-2)_\mu$), ignoring the dark matter relic density. We discuss the sensitivities of the fits to the $(g-2)_\mu$ and BR($b \to s\gamma$) constraints, contrasting fits with and without the $(g-2)_\mu$ constraint, and combining the theoretical and experimental errors for BR($b \to s\gamma$) linearly or in quadrature. We present predictions for $m_{\tilde{g}}$, BR($B_s \to \mu^+\mu^-$), M_h and M_A, and update predictions for spin-independent dark matter scattering, incorporating the uncertainty in the π-nucleon σ term $\Sigma_{\pi N}$. Finally, we present predictions based on our fits for the likely thresholds for sparticle pair production in e^+e^- collisions in the CMSSM and NUHM1.

KCL-PH-TH/2011-28, LCTS/2011-14, CERN-PH-TH/2011-220,
DCPT/11/108, DESY 11-161, IPPP/11/54, FTPI-MINN-11/23, UMN-TH-3013/11

1. Introduction

In a series of papers, we and others have reported the results of global fits to pre-LHC [1–6] and LHC 2010 data [7–10] in the frameworks of simplified variants of the minimal supersymmetric extension of the Standard Model (MSSM) [11] with universal supersymmetry-breaking mass parameters at the GUT scale. We consider a class of models in which R-parity is conserved and the lightest supersymmetric particle (LSP), assumed to be the lightest neutralino $\tilde{\chi}_1^0$ [12], provides the cosmological cold dark matter [13]. The specific models studied have included the constrained MSSM (CMSSM) [14], with parameters m_0, $m_{1/2}$ and A_0 denoting common scalar, fermionic and trilinear soft supersymmetry-breaking parameters at the GUT scale, and $\tan\beta$ denoting the ratio of the two vacuum expectation values of the two Higgs fields. Other models studied include a model in which common supersymmetry-breaking contributions to the Higgs masses are allowed to be non-universal (the NUHM1) [15], a very constrained model in which trilinear and bilinear soft supersymmetry-breaking parameters are related (the VCMSSM) [16], and minimal supergravity (mSUGRA) [16,17] in which the gravitino mass is required to be the same as the universal soft supersymmetry-breaking scalar mass before renormalization.

The impressive increase in the accumulated LHC luminosity combined with the rapid analyses of LHC data by the ATLAS [18,19], CMS [20–22] and LHCb Collaborations [23] is putting increasing pressure on these and other supersymmetric models, in the continuing absence of any signal for supersymmetry. In this paper we update our previous frequentist fits [8,9] to include the analyses of ~ 1/fb of LHC data made public in July and August 2011 at the EPS HEP and Lepton-Photon Conferences, termed here $\mathrm{LHC}_{1/\mathrm{fb}}$, and also discuss the impact of the result on $\mathrm{BR}(B_s \to \mu^+\mu^-)$ by the CDF Collaboration [24]. As in [8], we also incorporate the results of the direct search for dark matter scattering by the XENON100 Collaboration [25] [1].

The approach we use has been documented in our previous papers [1–5, 7, 8], so we do not describe it in detail here, concentrating on relevant new aspects. We construct a global likelihood function that receives contributions from the standard portfolio of electroweak precision observables, as well as B-decay measurements such as $\mathrm{BR}(b \to s\gamma)$ and $\mathrm{BR}(B_u \to \tau\nu_\tau)$. The contributions to the likelihood function from $\mathrm{BR}(B_s \to \mu^+\mu^-)$, the XENON100 direct search for dark matter scattering and the LHC searches for supersymmetric signals are calculated within the `MasterCode` framework [9]. Concerning the theoretical predictions for the different observables, the `MasterCode` framework incorporates a code for the electroweak observables based on [26] as well as the `SoftSUSY` [27], `FeynHiggs` [28], `SuFla` [29], `SuperIso` [30], `MicrOMEGAs` [31] and `SSARD` [32] codes, using the SUSY Les Houches Accord [33]. The `MasterCode` framework is such that new observables can easily be incorporated via new 'afterburners', as we discuss below for the $\mathrm{LHC}_{1/\mathrm{fb}}$ constraints. We use a Markov Chain Monte Carlo (MCMC) approach to sample the parameter spaces of supersymmetric models, and the results of this paper are based on a basic resampling of the CMSSM with 70M points and a resampling of the NUHM1 with 70M additional points, both extending up to $m_0, m_{1/2} = 4000$ GeV.

Our results are based on the public results of searches for supersymmetric signals using ~ 1/fb of LHC data analyzed by the ATLAS and CMS Collaborations and ~ 0.3/fb of data analyzed by the LHCb Collaboration. For our purposes, some of the most important constraints are provided by the ATLAS [18] and CMS [20] searches for jets + $\not{E}_T$ events without leptons, as well as searches for the heavier MSSM Higgs bosons, H/A [19,21]. Also important are the new upper limits on $\mathrm{BR}(B_s \to \mu^+\mu^-)$ from the CMS [22], LHCb [23] and CDF Collaborations [24], which we incorporate in this paper as described below [2]. In this paper we focus on the analysis of the effects in the CMSSM and the NUHM1.

[1] Preliminary versions of these results were posted on [9] on July 25th, 2011.

[2] For other studies of recent data on $\mathrm{BR}(B_s \to \mu^+\mu^-)$ in supersymmetric frameworks, see [34].

As discussed briefly below, the VCMSSM and mSUGRA models are further disfavoured by the $\mathrm{LHC}_{1/\mathrm{fb}}$ data.

The absences of signals in the jets + $\not{E}_T$ searches disfavour the ranges of the model mass parameters $(m_0, m_{1/2})$ that had been favoured in our previous analyses of the CMSSM and NUHM1 [7, 8], and our current best fits have $m_0 \sim 150$ to 450 GeV and $m_{1/2} \sim 750$ GeV. Reconciling these larger values of $(m_0, m_{1/2})$ with $(g-2)_\mu$ favours values of $\tan\beta \sim 40$, though with a large uncertainty. The regions of parameter space with large $\tan\beta$ are constrained also by the new upper limits on $\mathrm{BR}(B_s \to \mu^+\mu^-)$, as well as the LHC H/A searches. Using our standard implementation of the $(g-2)_\mu$ constraint based on a Standard Model (SM) calculation [42], and combining the theoretical and experimental errors in $\mathrm{BR}(b \to s\gamma)$ in quadrature, we find that the p-value for the CMSSM best-fit point is now $\sim 15\%$, and that for the NUHM1 is $\sim 16\%$. On the other hand, we show that if the $(g-2)_\mu$ constraint is dropped much larger regions of the $(m_0, m_{1/2})$ and other parameter planes are allowed at the 68 and 95% CL, and these p-values increase to 38% in both models. In contrast, changing the treatment of $\mathrm{BR}(b \to s\gamma)$ by adding linearly the theoretical and experimental errors has relatively little impact on the fits and their p-values, increasing them both to 18%.

On the basis of these results, we present updated predictions for the gluino mass $m_{\tilde{g}}$, $\mathrm{BR}(B_s \to \mu^+\mu^-)$, and the light and heavy Higgs masses M_h and M_A. We also present updated predictions for the spin-independent dark matter scattering cross section, σ_p^{SI}, stressing the importance of the uncertainty in the π-nucleon σ term $\Sigma_{\pi N}$ [35].

In addition, we use our results to present likelihood functions for the thresholds for sparticle pair production in e^+e^- collisions. These results indicate that, within the CMSSM and NUHM1, the best-fit values for the sparticle thresholds lie above $E_{\mathrm{CM}} = 500$ GeV. However, we emphasize that these results are derived in the context of specific models with specific universal soft supersymmetry-breaking masses at the GUT scale, and do not apply to other classes of supersymmetric models.

2. Implementations of the New LHC Constraints

Jets + $\not{E}_T$ searches

The CMS and ATLAS Collaborations have both announced new exclusions in the $(m_0, m_{1/2})$ plane of the CMSSM based on searches for events with jets + $\not{E}_T$ unaccompanied by charged leptons, assuming $\tan\beta = 10$, $A_0 = 0$ and $\mu > 0$. The updated CMS α_T analysis is based on 1.1/fb of data [20], and the updated ATLAS 0-lepton analysis is based on 1.04/fb of data [18]. It is known that 0-lepton analyses are in general relatively insensitive to the $\tan\beta$ and A_0 parameters of the CMSSM, as has been confirmed specifically for the CMS α_T analysis, and they are also insensitive to the amount of Higgs non-universality in the NUHM1. Therefore, we treat these analyses as constraints in the $(m_0, m_{1/2})$ planes of the CMSSM and NUHM1 that are independent of the other model parameters. The ATLAS [36] and CMS Collaborations [37] have also announced new exclusions for searches for jets + $\not{E}_T$ events with one or more charged leptons with ~ 1/fb of data, but these have in general less expected sensitivity, and are more dependent on the other model parameters, so we do not include them in our analysis. A similar remark applies to the new ATLAS limits on events with b jets + $\not{E}_T$ unaccompanied by charged leptons using 0.83/fb of data [38] and on events with b jets + $\not{E}_T$ + 1 lepton using 1.03/fb of data [39] [3].

The CMS and ATLAS 0-lepton searches are more powerful in complementary regions of the $(m_0, m_{1/2})$ plane. Along each ray in this plane, we compare the expected CMS and ATLAS sensitivities, select the search that has the stronger expected 95% CL limit, and apply the constraint imposed by that search [4]. We assign $\Delta\chi^2 = 5.99$,

[3] It would facilitate the modelling of LHC constraints on SUSY if each Collaboration could combine the results from its different missing-energy searches, as is already done for Higgs searches.

[4] It would also facilitate the modelling of LHC constraints on supersymmetry if the results from different Collaborations were combined officially, as was done at LEP, is already done for $\mathrm{BR}(B_s \to \mu^+\mu^-)$ searches, and is planned

corresponding to 1.96 effective standard deviations, along the CMS and ATLAS 95% 0-lepton exclusion contours in the $(m_0, m_{1/2})$ plane. In the absence of more complete experimental information, we approximate the impact of these constraints by assuming that event numbers scale along rays in this plane $\propto \mathcal{M}^{-4}$ where $\mathcal{M} \equiv \sqrt{m_0^2 + m_{1/2}^2}$ (more details can be found in [8]). We then use these numbers to calculate the effective numbers of standard deviations and corresponding values of $\Delta\chi^2$ at each point in the plane.

Searches for heavy MSSM Higgs bosons

The CMS Collaboration has announced a new constraint on the heavy MSSM Higgs bosons from a search for the neutral bosons $H/A \to \tau^+\tau^-$ using 1.6/fb of data [21] and ATLAS has presented a similar constraint using 1.06/fb of data [19], the results being presented as 95% CL upper limits on the product of the production cross section times $\tau^+\tau^-$ branching ratio as a function of the common mass, $M_{H/A}$, for masses smaller than about 500 GeV. In our analysis we use the CMS constraint, which has the greater expected sensitivity. The CMS Collaboration has also announced a constraint on the decay chain $t \to H^+ \to \tau^+\nu$ using 1.09/fb of data [40], but this yields a constraint in a generic $(M_A, \tan\beta)$ plane that is much weaker than the above searches for H/A, so we do not implement it in our analysis.

We assign $\Delta\chi^2 = 3.84$, corresponding to 1.96 effective standard deviations, to model parameter sets predicting an H/A signal at the 95% CL given by the CMS constraint, for each fixed value of M_A. Other model parameter sets are assigned values of $\Delta\chi^2$ according to the numbers of effective standard deviations corresponding to the numbers of events they predict. For any fixed value of $M_{H/A}$, these event numbers scale approximately as $(\tan\beta)^2$.

Constraints on $\mathrm{BR}(B_s \to \mu^+\mu^-)$

Three new results on $\mathrm{BR}(B_s \to \mu^+\mu^-)$ have been announced recently. One is an excess of candidate $B_s \to \mu^+\mu^-$ events reported by the CDF Collaboration [24], which corresponds to $\mathrm{BR}(B_s \to \mu^+\mu^-) = (1.8^{+1.1}_{-0.9}) \times 10^{-8}$ or $\mathrm{BR}(B_s \to \mu^+\mu^-) < 4.0 \times 10^{-8}$ at the 95% CL. The other two new results are upper limits from the CMS Collaboration using 1.14/fb of data [22]: $\mathrm{BR}(B_s \to \mu^+\mu^-) < 1.9 \times 10^{-8}$ at the 95% CL, and from the LHCb Collaboration using 0.34/pb of data [23]: $\mathrm{BR}(B_s \to \mu^+\mu^-) < 1.5 \times 10^{-8}$ at the 95% CL.

These three results are reasonably compatible, though there is some tension between the CDF and CMS/LHCb results. The two latter collaborations have released an official combination of their results [41], which yields $\mathrm{BR}(B_s \to \mu^+\mu^-) < 1.08 \times 10^{-8}$ at the 95% CL. In our implementation of the $\mathrm{BR}(B_s \to \mu^+\mu^-)$ constraint, we use $\Delta\chi^2$ corresponding to the full likelihood function provided by this combination, which has a global minimum close to the SM prediction. We also comment on the changes in our results that would follow from an (unofficial) combination with the CDF result [24], which would yield a $\Delta\chi^2$ function with a minimum at $\mathrm{BR}(B_s \to \mu^+\mu^-)$ at about twice the SM value.

Constraints on dark matter scattering

We incorporate the upper limit on the spin-independent dark matter scattering cross section σ_p^{SI} provided by the XENON100 Collaboration [25] in a similar manner to [8]. In that paper we discussed extensively the uncertainty in the spin-independent scattering matrix element induced by the relatively ill-determined value of the π-nucleon σ term, $\Sigma_{\pi N}$. In this paper we use $\Sigma_{\pi N} = 50 \pm 14$ MeV, and neglect other uncertainties, e.g., in modelling the dark matter distribution. We also do not consider here other experiments reporting signatures that would require σ_p^{SI} above the XENON100 limit. Nor do we consider limits on spin-dependent dark matter scattering and astrophysical signatures of dark matter annihilations, which currently do not constrain the CMSSM and NUHM1 [8].

for Higgs searches.

3. Results

The $(m_0, m_{1/2})$ planes in the CMSSM and NUHM1

Fig. 1 displays contours with $\Delta\chi^2 = 2.30$ (red) and 5.99 (blue) relative to the minimum values of χ^2 at the best-fit points (denoted by green stars) in the $(m_0, m_{1/2})$ planes for the CMSSM and NUHM1 [5]. Such contours are commonly interpreted as 68 and 95% CL contours. The solid lines are the contours after incorporation of the $\mathrm{LHC}_{1/\mathrm{fb}}$ results, and the dotted lines are the CL contours obtained from an analysis of the pre-LHC and pre-XENON100 data [5]. Consequently, the differences in the contours show the *full* impact of the $\sim 1/\mathrm{fb}$ data set of LHC data. The crinkles in these contours give an indication of the sampling uncertainties in our analysis.

We see that the new best-fit points with $(m_0, m_{1/2}) = (450, 780)$ GeV in the CMSSM and $(150, 730)$ GeV in the NUHM1 (denoted by solid green stars) lie well within the previous 95% CL region. On the other hand, the pre-LHC best-fit points with $(m_0, m_{1/2}) = (90, 360)$ GeV in the CMSSM and $(110, 340)$ GeV in the NUHM1 (denoted by open stars), lie far outside the regions allowed by the $\mathrm{LHC}_{1/\mathrm{fb}}$ data. Thus, we see that there is now significant tension between the $\mathrm{LHC}_{1/\mathrm{fb}}$ and pre-LHC data sets. The full set of parameters of the post-$\mathrm{LHC}_{1/\mathrm{fb}}$ and pre-LHC best-fit points are shown in Table 1 [6].

In both the CMSSM and the NUHM1, as we discuss later, the 68% CL upper limits on $m_{1/2}$ in Fig. 1 are largely driven by $(g-2)_\mu$, and the 95% CL upper limits are largely driven by the relic density constraint, with large-$m_{1/2}$ points lying in the heavy-Higgs rapid-annihilation funnel at large $\tan\beta$. The fact that much larger regions in the $(m_0, m_{1/2})$ are now allowed at the 95% CL, as compared to the pre-LHC fit, indicates that the tension between $(g-2)_\mu$, favouring relatively low SUSY scales, and the direct search limits, favouring larger SUSY scales, has significantly reduced the sensitivity of the fits within the CMSSM and the NUHM1 for constraining the SUSY parameters. Since the χ^2 values of the best-fit points are significantly higher (see Table 1), and consequently the χ^2 distribution towards higher values of m_0 and $m_{1/2}$ is much flatter than in the pre-LHC case, the precise location of the 68% and 95% CL contours is less precisely determined than before. The narrower range of m_0 allowed in the NUHM1 at the 68% CL, compared to the CMSSM, is due to the appearance of a 'pit' with a lower absolute value of χ^2 that is attainable in this model thanks to its flexibility in reconciling the $(g-2)_\mu$ with the $\tilde{\chi}_1^0$ LSP and other constraints by deviating from Higgs mass universality. As in our previous analysis including 2010 LHC and XENON100 data [8], we find no distinct enhancement of the likelihood in the focus-point region at large m_0.

The absolute values of χ^2 at the best-fit points for the pre-LHC case and for the $\mathrm{LHC}_{1/\mathrm{fb}}$ data set using our standard implementations of the $(g-2)_\mu$ and $\mathrm{BR}(b \to s\gamma)$ constraints are given in Table 1. Our updated analysis of the pre-LHC data set yields $\chi^2/\mathrm{d.o.f.} = 21.5/20 (20.8/18)$ in the CMSSM and NUHM1, respectively, corresponding to p-values of 37% and 29%. On the other hand, using the $\mathrm{LHC}_{1/\mathrm{fb}}$ data set, we find that the minimum values of χ^2 are significantly larger than the numbers of effective degrees of freedom in the fits, which are also shown in Table 1: $\chi^2/\mathrm{d.o.f.} = 28.8/22\,(27.3/21)$ for the CMSSM and NUHM1, respectively [7]. Correspondingly, the best fits have significantly reduced probability values, $\sim 15\%$ in the CMSSM and $\sim 16\%$ in the NUHM1 [8]. If we combine the

[5] The NUHM1 analysis includes both the dedicated NUHM1 sample, which is efficient for smaller values of $(m_0, m_{1/2})$, and the basic set of CMSSM points, which provide extra NUHM1 sampling at larger values of $(m_0, m_{1/2})$.

[6] The parameters of the pre-LHC best-fit CMSSM and NUHM1 points given in Table 1 differ by up to 1 σ from those given in [8]. These differences are caused primarily by changes in the data inputs.

[7] For technical reasons, the Γ_Z constraint was not included in our previous fits, leading to changes of one unit in the numbers of effective degrees of freedom in the fits.

[8] The p-values for the VCMSSM and mSUGRA are somewhat smaller, as was found previously [8]: $\chi^2/\mathrm{d.o.f.} = 31.2/23 (32.5/23)$, respectively, corresponding to p-values of 12% and 9%. We do not discuss these models further, except to comment that the light-Higgs funnel region found previously in these models is now excluded by ATLAS data [18], in particular.

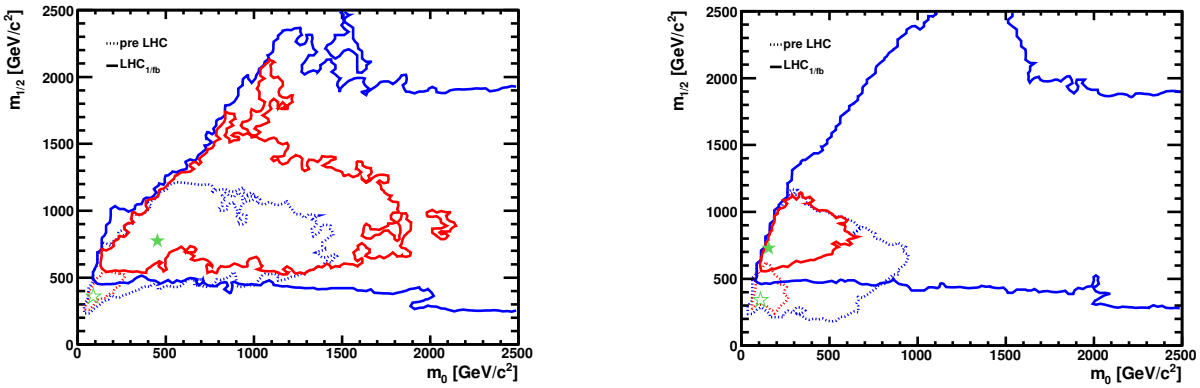

Figure 1. *The $(m_0, m_{1/2})$ planes in the CMSSM (left) and the NUHM1 (right). In each plane, the best-fit point after incorporation of the LHC$_{1/\mathrm{fb}}$ constraints is indicated by a filled green star, and the pre-LHC fit [5] by an open star. The $\Delta\chi^2 = 2.30$ and 5.99 contours, commonly interpreted as the boundaries of the 68 and 95% CL regions, are indicated in red and blue, respectively, the solid lines including the LHC$_{1/\mathrm{fb}}$ data and the dotted lines showing the pre-LHC fits.*

BR($b \to s\gamma$) errors linearly instead of quadratically, the values of χ^2 decrease by 0.8(0.7) in the CMSSM and NUHM1, respectively, and the p-values increase modestly to 18% in both cases. On the other hand, if we drop the $(g-2)_\mu$ constraint, we find χ^2/d.o.f = 21.3/20(20.3/19), respectively, corresponding to p-values of 38% in both cases. Thus, the qualities of our best fits are not very sensitive to the treatment of BR($b \to s\gamma$), but are much more sensitive to the inclusion of $(g-2)_\mu$, as we discuss later in more detail.

The degrees of non-universality, $r \equiv m_H^2/m_0^2$, for the best-fit NUHM1 points in Table 1 are as follows: $r = -57$ (pre-LHC), $r = -54$ (LHC$_{1/\mathrm{fb}}$), $r = -54$ (linear BR($b \to s\gamma$) error combination), $r = -0.39$ (dropping $(g-2)_\mu$ constraint), $r = -0.39$ (including both variants). Since r is quite poorly constrained, we do not quote its uncertainties.

We note that the best-fit values of M_h are significantly higher in the CMSSM and NUHM1 fits dropping $(g-2)_\mu$, with their large values of $(m_0, m_{1/2})$, than in the fits that include the $(g-2)_\mu$ constraint. An LHC measurement of M_h could provide a diagnostic discriminating between models with light and heavy spectra of third-generation squarks, and help forecast the likelihood of discovering these sparticles in future LHC runs. Within the CMSSM and NUHM1, measuring M_h could advise us whether to take $(g-2)_\mu$ at face value or, conversely, hint towards extensions of those models.

Table 2 displays the contributions to the total χ^2 of each of the observables at the best-fit points in the CMSSM and NUHM1, revealing where this tension originates. We note, as already mentioned above, that there is an important contribution to the χ^2 function coming from the $(g-2)_\mu$ constraint, as well as the LHC$_{1/\mathrm{fb}}$ constraints. We return later to a more complete discussion of the tension between these constraints, and also of the treatment of the BR($b \to s\gamma$) constraint.

Table 2 also displays a similar χ^2 breakdown evaluated assuming the central values of $m_t, \Delta\alpha^{(5)}_{\mathrm{had}}(M_Z)$ and M_Z for a CMSSM point at very large $(m_0, m_{1/2}) = (15, 15)$ TeV, $A_0 = 100$ GeV and $\tan\beta = 10$, near the limit in which its predictions coincide with those of the SM for the same value of M_h. This is very similar to the global best-fit value of M_h in the SM obtained incorporating the limits from the direct

Model	Minimum χ^2/d.o.f.	Prob-ability	$m_{1/2}$ (GeV)	m_0 (GeV)	A_0 (GeV)	$\tan\beta$	M_h (GeV) (no LEP)
CMSSM pre-LHC	21.5/20	37%	360^{+180}_{-100}	90^{+220}_{-50}	-400^{+730}_{-970}	15^{+15}_{-9}	$111.5^{+3.5}_{-1.2}$
CMSSM $\mathrm{LHC}_{1/\mathrm{fb}}$	28.8/22	15%	780^{+1350}_{-270}	450^{+1700}_{-320}	-1100^{+3070}_{-3680}	41^{+16}_{-32}	$119.1^{+3.4}_{-2.9}$
Linear Δ BR($b \to s\gamma$)	28.0/22	18%	720^{+1170}_{-230}	420^{+1270}_{-270}	-1100^{+2180}_{-2750}	39^{+18}_{-22}	$118.6^{+3.9}_{-1.9}$
$(g-2)_\mu$ neglected	21.3/20	38%	2000^{+}_{-}	1050^{+}_{-}	430^{+}_{-}	22^{+}_{-}	$124.8^{+3.4}_{-10.5}$
Both	20.5/20	43%	1880^{+}_{-}	1340^{+}_{-}	1890^{+}_{-}	47^{+}_{-}	$126.1^{+2.1}_{-6.3}$
NUHM1 pre-LHC	20.8/18	29%	340^{+280}_{-110}	110^{+160}_{-30}	520^{+750}_{-1730}	13^{+27}_{-6}	$118.9^{+1.1}_{-11.4}$
NUHM1 $\mathrm{LHC}_{1/\mathrm{fb}}$	27.3/21	16%	730^{+630}_{-170}	150^{+450}_{-50}	-910^{+2990}_{-1170}	41^{+16}_{-24}	$118.8^{+2.7}_{-1.1}$
Linear Δ BR($b \to s\gamma$)	26.6/21	18%	730^{+220}_{-90}	150^{+80}_{-20}	-910^{+2990}_{-1060}	41^{+16}_{-22}	$118.8^{+3.1}_{-1.3}$
$(g-2)_\mu$ neglected	20.3/19	38%	2020^{+}_{-}	1410^{+}_{-}	2580^{+}_{-}	48^{+}_{-}	$126.6^{+0.7}_{-1.9}$
Both	19.5/19	43%	2020^{+}_{-}	1410^{+}_{-}	2580^{+}_{-}	48^{+}_{-}	$126.6^{+0.7}_{-1.9}$

Table 1

Comparison of the best-fit points found in the CMSSM and NUHM1 pre-LHC (including the upper limit on $\mathrm{BR}(B_s \to \mu^+\mu^-)$ *available then), and with the* $\mathrm{LHC}_{1/\mathrm{fb}}$ *data set (also including the XENON100 constraint) using the standard implementations of the* $(g-2)_\mu$ *and BR*$(b \to s\gamma)$ *constraints, followed by variants first adding linearly the theoretical and experimental errors in BR*$(b \to s\gamma)$ *and then dropping* $(g-2)_\mu$*, and finally combining both variants. The errors for fits dropping* $(g-2)_\mu$ *are large and asymmetric, and are not indicated. The predictions for* M_h *do not include the constraint from the direct LEP Higgs search, and have an estimated theoretical error of* ± 1.5 GeV.

Higgs searches at LEP, the Tevatron and the LHC [59]. Using the SM limit of the CMSSM within the `MasterCode` framework ensures that this evaluation of χ^2 in the "SM" can be compared directly with those at the best-fit points in the CMSSM and NUHM1. In the "SM" case we discard the constraints imposed by the cosmological dark matter density and XENON100, since there is no way to explain dark matter with the SM. We also discard the LHC missing-energy and H/A constraints, but all other constraints are kept. Consequently, we *do* list the contribution to χ^2 from $(g-2)_\mu$. If this is included (omitted), the global χ^2 for the "SM" is 32.7 (21.5). The number of degrees of freedom for the "SM" is consequently 23 (22) and the p-value is 9% (49%). We observe that the p-value for the CMSSM is rather larger than that for the "SM" if $(g-2)_\mu$ is included, though similar if $(g-2)_\mu$ is not included in the "SM" and MSSM analyses.

We also note that one of the big contributors to the global χ^2 functions for all the models is $A_{\mathrm{fb}}(b)$, which contributes $\Delta\chi^2 \sim 7$ to each of the fits, suppressing all their p-values. Prior to the LHC results, the CMSSM yielded a significant improvement to χ^2, with the dominant contribution coming from $(g-2)_\mu$ ($\Delta\chi^2 = -10.8$). Other contributing observables were M_W ($\Delta\chi^2 = -1.6$) and A_ℓ(SLD) ($\Delta\chi^2 = -1.3$), though $A_{\mathrm{fb}}(b)$ was somewhat worse in the CMSSM ($\Delta\chi^2 = 2.1$). The post-LHC comparison with the "SM" is shown in Table 2. Looking at the entries for the electroweak precision observables, the only significant change is now that for $(g-2)_\mu$($\Delta\chi^2 = -6.8$), with all other observables showing changes $|\Delta\chi^2| < 1$. Thus, when $(g-2)_\mu$is dropped as a constraint, the resulting χ^2 for the best-fit points in the CMSSM and "SM" are very similar. In

Observable	Source Th./Ex.	Constraint	$\Delta\chi^2$ (CMSSM)	$\Delta\chi^2$ (NUHM1)	$\Delta\chi^2$ ("SM")
m_t [GeV]	[43]	173.2 ± 0.90	0.05	0.06	-
$\Delta\alpha^{(5)}_{\rm had}(M_Z)$	[42]	0.02749 ± 0.00010	0.009	0.004	-
M_Z [GeV]	[44]	91.1875 ± 0.0021	2.7×10^{-5}	0.26	-
Γ_Z [GeV]	[26] / [44]	$2.4952 \pm 0.0023 \pm 0.001_{\rm SUSY}$	0.078	0.047	0.14
$\sigma^0_{\rm had}$ [nb]	[26] / [44]	41.540 ± 0.037	2.50	2.57	2.54
R_l	[26] / [44]	20.767 ± 0.025	1.05	1.08	1.08
$A_{\rm fb}(\ell)$	[26] / [44]	0.01714 ± 0.00095	0.72	0.69	0.81
$A_\ell(P_\tau)$	[26] / [44]	0.1465 ± 0.0032	0.11	0.13	0.07
$R_{\rm b}$	[26] / [44]	0.21629 ± 0.00066	0.26	0.29	0.27
$R_{\rm c}$	[26] / [44]	0.1721 ± 0.0030	0.002	0.002	0.002
$A_{\rm fb}(b)$	[26] / [44]	0.0992 ± 0.0016	7.17	7.37	6.63
$A_{\rm fb}(c)$	[26] / [44]	0.0707 ± 0.0035	0.86	0.88	0.80
A_b	[26] / [44]	0.923 ± 0.020	0.36	0.36	0.35
A_c	[26] / [44]	0.670 ± 0.027	0.005	0.005	0.005
A_ℓ(SLD)	[26] / [44]	0.1513 ± 0.0021	3.16	3.03	3.51
$\sin^2\theta^\ell_{\rm w}(Q_{\rm fb})$	[26] / [44]	0.2324 ± 0.0012	0.63	0.64	0.59
M_W [GeV]	[26] / [44]	$80.399 \pm 0.023 \pm 0.010_{\rm SUSY}$	1.77	1.39	2.08
$a_\mu^{\rm EXP} - a_\mu^{\rm SM}$	[53] / [42,54]	$(30.2 \pm 8.8 \pm 2.0_{\rm SUSY}) \times 10^{-10}$	4.35	1.82	11.19 (N/A)
M_h [GeV]	[28] / [55,56]	$> 114.4[\pm1.5_{\rm SUSY}]$	0.0	0.0	0.0
$\mathrm{BR}^{\rm EXP/SM}_{\rm b\to s\gamma}$	[45] / [46]	$1.117 \pm 0.076_{\rm EXP}$ $\pm0.082_{\rm SM} \pm 0.050_{\rm SUSY}$	1.83	1.09	0.94
$\mathrm{BR}(B_s \to \mu^+\mu^-)$	[29] / [41]	CMS & LHCb	0.04	0.44	0.01
$\mathrm{BR}^{\rm EXP/SM}_{\rm B\to\tau\nu}$	[29] / [46]	$1.43 \pm 0.43_{\rm EXP+TH}$	1.43	1.59	1.00
$\mathrm{BR}(B_d \to \mu^+\mu^-)$	[29] / [46]	$< 4.6[\pm0.01_{\rm SUSY}] \times 10^{-9}$	0.0	0.0	0.0
$\mathrm{BR}^{\rm EXP/SM}_{B\to X_s\ell\ell}$	[47]/ [46]	0.99 ± 0.32	0.02	$\ll 0.01$	$\ll 0.01$
$\mathrm{BR}^{\rm EXP/SM}_{K\to\mu\nu}$	[29] / [48]	$1.008 \pm 0.014_{\rm EXP+TH}$	0.39	0.42	0.33
$\mathrm{BR}^{\rm EXP/SM}_{K\to\pi\nu\bar\nu}$	[49]/ [50]	< 4.5	0.0	0.0	0.0
$\Delta M^{\rm EXP/SM}_{B_s}$	[49] / [51,52]	$0.97 \pm 0.01_{\rm EXP} \pm 0.27_{\rm SM}$	0.02	0.02	0.01
$\frac{\Delta M^{\rm EXP/SM}_{B_s}}{\Delta M^{\rm EXP/SM}_{B_d}}$	[29] / [46,51,52]	$1.00 \pm 0.01_{\rm EXP} \pm 0.13_{\rm SM}$	$\ll 0.01$	0.33	$\ll 0.01$
$\Delta\epsilon^{\rm EXP/SM}_K$	[49] / [51,52]	$1.08 \pm 0.14_{\rm EXP+TH}$	0.27	0.37	0.33
$\Omega_{\rm CDM}h^2$	[31] / [13]	$0.1120 \pm 0.0056 \pm 0.012_{\rm SUSY}$	8.4×10^{-4}	0.1	N/A
$\sigma_p^{\rm SI}$	[25]	$(m_{\tilde\chi^0_1}, \sigma_p^{\rm SI})$ plane	0.13	0.13	N/A
jets + $\not{E}_T$	[18,20]	$(m_0, m_{1/2})$ plane	1.55	2.20	N/A
$H/A, H^\pm$	[21]	$(M_A, \tan\beta)$ plane	0.0	0.0	N/A
Total χ^2/d.o.f. p-values	All	All	28.8/22 15%	27.3/21 16%	32.7/23 (21.5/22) 9% (49%)

Table 2

List of experimental constraints used in this work, including experimental and (where applicable) theoretical errors: supersymmetric theory uncertainties in the interpretations of one-sided experimental limits are indicated by [...]. Also shown are the contributions that these constraints make to the total χ^2 functions at the best-fit points in the CMSSM and NUHM1, respectively, and (for comparison) in the SM limit of the CMSSM (called "SM") including (excluding) $(g-2)_\mu$. The total values of χ^2, the numbers of degrees of freedom and the p-values at these points are shown in the two bottom rows.

the case of the post-LHC NUHM1, we also see a large drop in χ^2 relative to the "SM" due to $(g-2)_\mu (\Delta\chi^2 = -9.4)$ and again all others give $|\Delta\chi^2| < 1$. We also note that in both the CMSSM and NUHM1 the best fits receive significant contributions from the LHC $\not{E}_T$ + jets searches.

To illustrate further the impact of $\mathrm{LHC}_{1/\mathrm{fb}}$ experimental constraints relative to pre-LHC preferred regions, we display in Fig. 2 colour-coded contours of approximate[9] p-values from our global fits for the CMSSM and NUHM1. Care is taken to count the effective number of degrees of freedom at each point, considering all constraints that contribute non-trivially to the χ^2 functions. Thus, for example, we drop the contribution of the $\mathrm{LHC}_{1/\mathrm{fb}}$ missing-energy constraints where they contribute $\Delta\chi^2 < 0.1$, causing the visible changes in shading along drooping diagonal lines in both panels of Fig. 2. (This cut is applied *only* to the $\mathrm{LHC}_{1/\mathrm{fb}}$ missing-energy constraint.) Substantial non-zero p-values are observed to extend to high m_0 and $m_{1/2}$, in both pre- (upper panels) and post-$\mathrm{LHC}_{1/\mathrm{fb}}$ (lower panels), and both the CMSSM (left panels) and NUHM1 (right panels) models. As also seen earlier, the primary effect of the $\mathrm{LHC}_{1/\mathrm{fb}}$ searches for jets + $\not{E}_T$ is most evident for $m_{1/2}$, preferring higher values than that predicted by the pre-LHC global fits. At even higher (m_0, $m_{1/2}$), beyond the drooping diagonal line, slight increases in approximate p-values appear when comparing the pre-LHC results with the post-$\mathrm{LHC}_{1/\mathrm{fb}}$ and post XENON100 results. This is due partly to the experimental constraint on $\mathrm{BR}(B_s \to \mu^+\mu^-)$, which is nearing the SM prediction. Regions of the CMSSM and NUHM1 parameter spaces approaching the high-mass decoupling limit receive a non-zero contribution from $\mathrm{BR}(B_s \to \mu^+\mu^-)$ in the post-$\mathrm{LHC}_{1/\mathrm{fb}}$ era, resulting in $\Delta\chi^2 < 1$, which actaually improves the overall χ^2 per effective degree of freedom. Additionally, the XENON100 constraint slightly prefers high mass scales, so as to accomodate the small "excess" in events, also resulting in slightly better values of χ^2 per effective degree of freedom.

Complementing the comparison of the p-values of the "SM", the CMSSM and the NUHM1, we now use the standard F-test to test the utility of adding one or several parameters to a model fit of data. Given a set of data comprising N observables and a model using m parameters, one may compute $\chi^2(m)$ for $N-m$ degrees of freedom as done above. In general, adding r parameters produces a reduced value of $\chi^2(m+r)$, and the difference between these two χ^2 distributions is itself a χ^2 distribution for r degrees of freedom. The F-statistic is defined by

$$F_\chi \equiv \frac{\chi^2(m) - \chi^2(m+r)}{\chi^2(m+r)/(N-m-r)} > 0. \qquad (1)$$

The probability that introducing the r new parameters are warranted is found by integrating the F-distribution, $p_F(f, r, N-m-r)$, from $f = F_\chi$ to ∞. We use the F-test to illustrate the relative preference for various models.

In our case, for the "SM" we have $\chi^2 = 32.7(21.5)$ for 23 (22) degrees of freedom if $(g-2)_\mu$ is included in (omitted from) the fit. Using the CMSSM value of $\chi^2 = 28.8$ for 22 degrees of freedom, we find $F_\chi = 2.98$, and the probability that switching to the CMSSM is warranted is $p_F = 90\%$. Correspondingly, using the NUHM1 value of $\chi^2 = 27.3$ for 21 degrees of freedom, we find $F_\chi = 4.15$, and the probability that switching to the NUHM1 is warranted is $p_F = 97\%$. We can also compare the improvement in χ^2 gained by moving from the CMSSM to the NUHM1. In this case the probability that the extra parameter needed to define the NUHM1 model is preferred over the CMSSM case is 71%. Fig. 3 uses shading to display values of p_F in the $(m_0, m_{1/2})$ planes of the CMSSM and NUHM1. On the basis of these plots, we find that present data may warrant switching from the "SM" to the CMSSM or NUHM1 for values of $m_{1/2}$ out to ~ 1500 GeV [10]. Beyond this range of $m_{1/2}$, the

[9] Strictly speaking, transforming a χ^2 value to a p-value, using a specified number of degrees of freedom, is valid for Gaussian-behaved constraints. Because some of the experimental limits are one-sided and modelled in a non-Gaussian manner as previously described, the p-values reported here can therefore only be considered approximate.

[10] We note, however, that these results may be too favourable to the CMSSM or NUHM1, since they do not include the impacts of the many lower-sensitivity con-

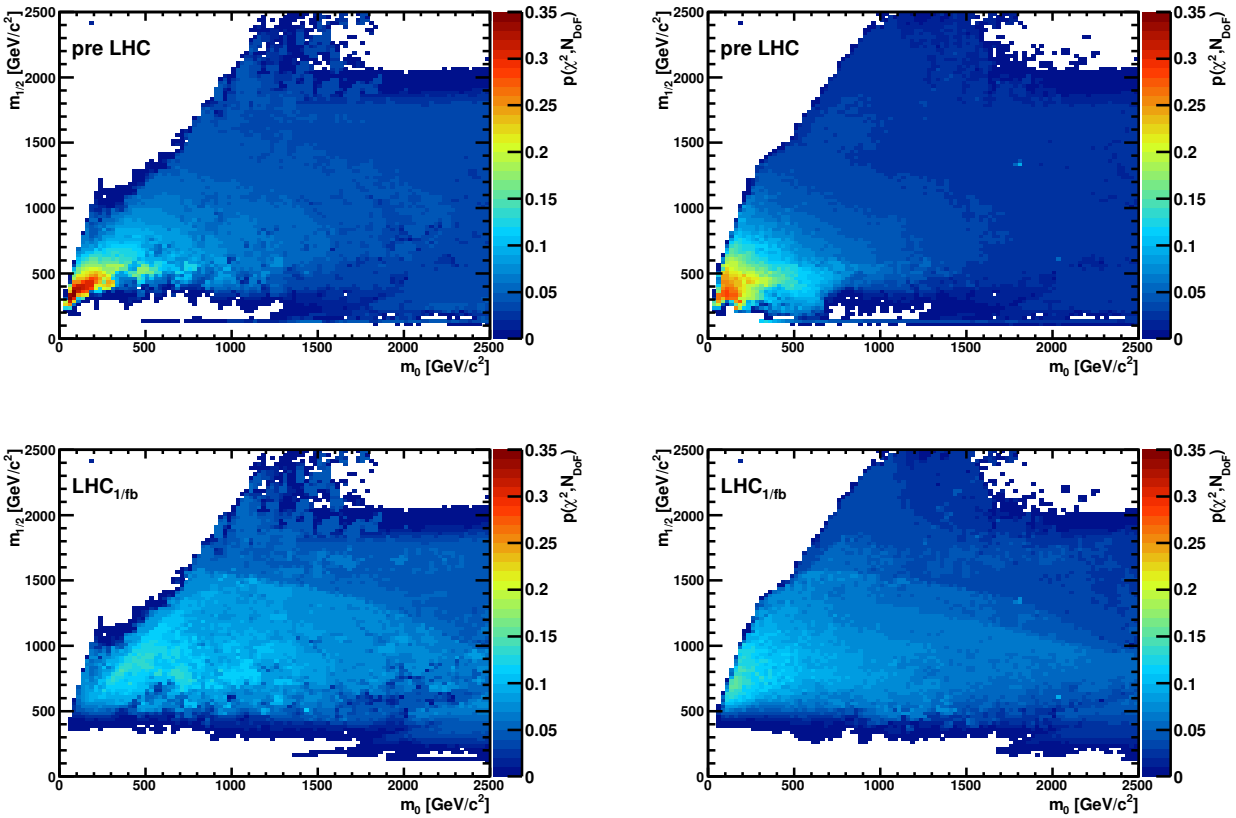

Figure 2. *The $(m_0, m_{1/2})$ planes in the CMSSM (left) and the NUHM1 (right), for the pre-LHC data set (upper) and LHC$_{1/\mathrm{fb}}$ data set (lower). In each plane, different regions are colour-coded according to the p-values found in our global fits. We note that in the LHC$_{1/\mathrm{fb}}$ analysis the regions with $p > 0.05$ extend up to $m_{1/2} \sim 2000$ GeV in each case.*

motivations for these models would be significantly reduced. We also note that the F-test indicates that there would be no advantage in switching to the CMSSM or the NUHM1 if $(g-2)_\mu$ were to be dropped.

An important part of the motivation for low-scale supersymmetry is to alleviate the fine-tuning of the Higgs mass parameter in the Standard Model. However, the problem of fine-tuning returns if the supersymmetric mass scales become large [60]. The required amount of fine-tuning is increased significantly in our LHC$_{1/\mathrm{fb}}$ fits compared to our pre-LHC fits, principally because of the increases in the best-fit values of m_0 and $m_{1/2}$. Specifically, in the CMSSM our best pre-LHC fit required fine-tuning by a factor ~ 100, whereas our best LHC$_{1/\mathrm{fb}}$ fit requires fine-tuning by a factor ~ 300. The corresponding numbers for the NUHM1 are ~ 250 pre-LHC and ~ 600 with the LHC$_{1/\mathrm{fb}}$ data.

Uncertainties in the analysis

In assessing the compatibility of the CMSSM and the NUHM1 with the experimental data it

straints from CMS and ATLAS. This problem could be avoided if the Collaborations publish official combinations of the sensitivities of their searches.

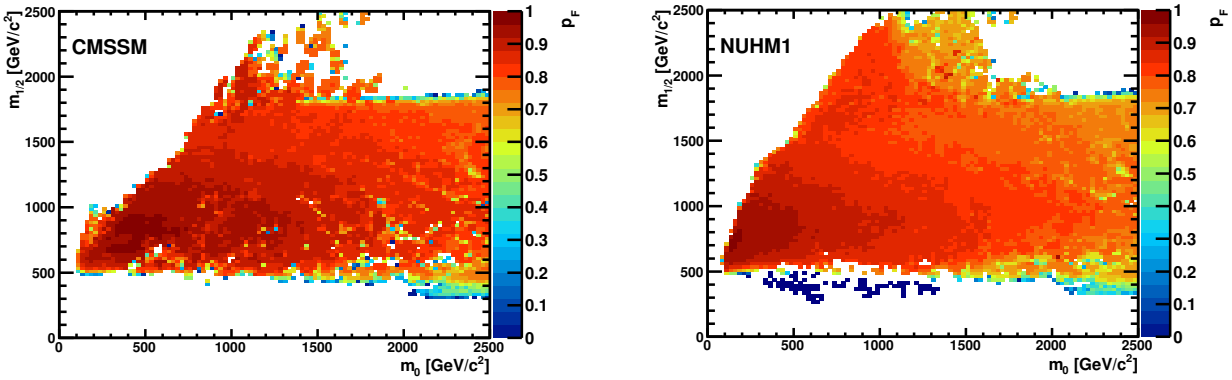

Figure 3. *The $(m_0, m_{1/2})$ planes in the CMSSM (left) and the NUHM1 (right). In each plane, different regions are colour-coded according to the values of p_F found by applying the F-test to our global fits. We note that the regions with $p_F > 0.8$ extend up to $m_{1/2} \sim 1500$ GeV in each case.*

is important also to examine carefully the most important systematic uncertainties in the constraints that drive the fit in this global likelihood analysis. We saw in the Table 2 that the most important contributions to the global χ^2 functions at the best-fit points in these models originate from the $(g-2)_\mu$ and $\mathrm{LHC}_{1/\mathrm{fb}}$ constraints. Exploring this further, Fig. 4 displays the CMSSM and NUHM1 $(m_0, m_{1/2})$ planes again, exhibiting the contribution to χ^2 from the $(g-2)_\mu$ constraint, evaluated for the model parameter sets that minimize the total χ^2 at each point in the plane. Their shapes are different in the CMSSM and NUHM1, reflecting the existence of the previously-mentioned 'pit' in the latter model where χ^2 may be reduced by some judicious choice of the degree of Higgs non-universality. *Prima facie*, there is tension between the $(g-2)_\mu$ constraint, which prefers small values of $(m_0, m_{1/2})$, and the $\mathrm{LHC}_{1/\mathrm{fb}}$ constraints, which prefer larger values of $(m_0, m_{1/2})$. This tension is alleviated for larger values of $\tan\beta$, which is why post-2010-LHC [8] and post-$\mathrm{LHC}_{1/\mathrm{fb}}$ fits have favoured larger values of $\tan\beta$ than pre-LHC fits [5], albeit with large uncertainties.

Fig. 5 again displays the $(m_0, m_{1/2})$ planes in the CMSSM (left) and the NUHM1 (right), this time showing as solid lines the 68% and 95% CL contours obtained by dropping the $(g-2)_\mu$ constraint, the contours obtained applying the $(g-2)_\mu$ constraint as in Fig. 1 being shown here for comparison as dotted lines. We see that, in the absence of the $(g-2)_\mu$ constraint, the outer parts of the 68% CL contours are expanded outwards, close to the 95% CL contours that are themselves close to the boundary set by the $\Omega_{\tilde{\chi}_1^0} h^2$ constraint [11]. Within the overall range allowed by this constraint, the most important constraint is that provided by the LHC data. We note that the global likelihood functions in the CMSSM and NUHM1 are very flat, and that the best-fit points found dropping the $(g-2)_\mu$ constraints are correspondingly quite uncertain. However, it is clear that the amounts of fine-tuning at $(g-2)_\mu$-less best-fit points are much higher than if $(g-2)_\mu$ is included.

We also comment on the treatment of $\mathrm{BR}(b \to s\gamma)$, where different points of view have been taken concerning the combination of the theo-

[11] This constraint is not sacrosanct, but could be relaxed by postulating some amount of R-violation, or some other source of dark matter, or by modifying the expansion history of the Universe, e.g., by altering the expansion rate during freeze-out, or by postulating some subsequent injection of entropy.

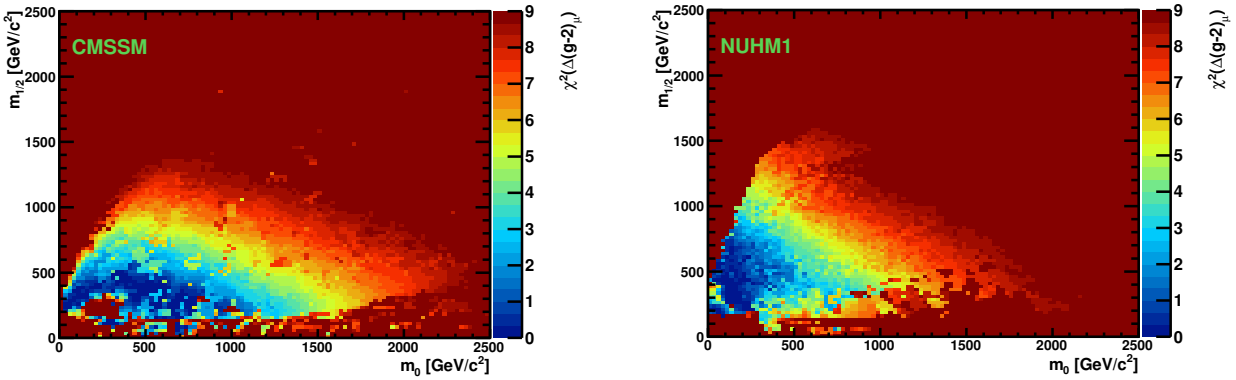

Figure 4. *The $(m_0, m_{1/2})$ planes in the CMSSM (left) and the NUHM1 (right), with shading displaying the contribution to the global χ^2 function from $(g-2)_\mu$ as calculated using low-energy e^+e^- data to evaluate the SM contribution. These contributions are evaluated for the parameter sets that minimize χ^2 at each point in the planes.*

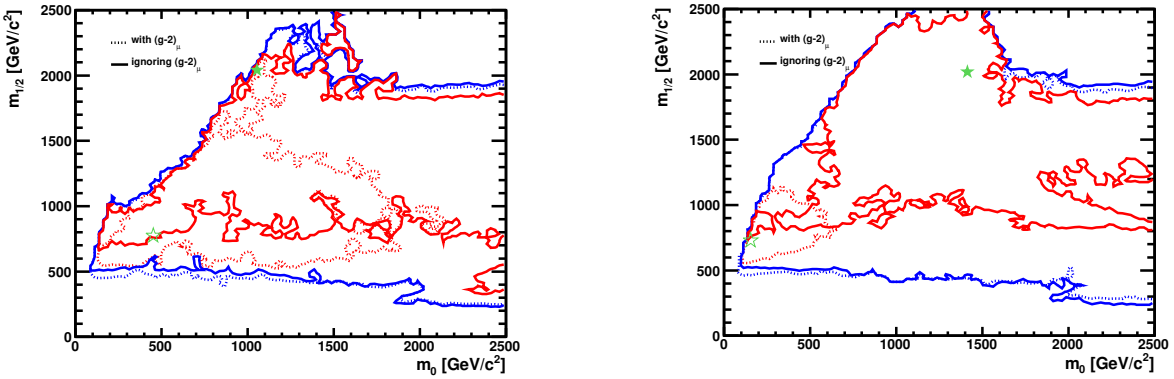

Figure 5. *The $(m_0, m_{1/2})$ planes in the CMSSM (left) and the NUHM1 (right). Here we show as solid lines the 68% and 95% CL contours obtained by dropping the $(g-2)_\mu$ constraint. The contours obtained applying the $(g-2)_\mu$ constraint as in Fig. 1 are shown here for comparison as dotted lines.*

retical and experimental errors [12]. The two uncertainties are of similar size, and the issue of how they are combined is more severe than for other observables. In our default implementation of BR($b \to s\gamma$) we add the quoted errors in

[12] As in our previous analyses, we do not take into account constraints from exclusive $b \to s\gamma$ transitions. In particular, we do not impose any constraint on the SUSY parameter space from the isospin asymmetry in $B \to K^*\gamma$, as included for instance in the `SuperIso` package [30]. A conservative treatment of non-factorizable contributions to this observable suggests a SM error exceeding ± 0.05, i.e., a relative error exceeding 100% (see, e.g., [61]), and even larger errors are associated to the contributions of non-SM operators (see, e.g., [62]). These uncertainties obscure possible SUSY contributions within the ranges currently of interest in the CMSSM and the NUHM1 models.

quadrature. However, it might be argued that the theoretical error should be regarded as an overall range of uncertainty that cannot be treated as an effective Gaussian error to be added in quadrature to the experimental error. Therefore, we consider as an alternative implementation of BR($b \to s\gamma$) the possibility of adding linearly the theoretical and experimental errors. As seen in Fig. 6, the region of the CMSSM $(m_0, m_{1/2})$ plane that is favoured at the 68% CL *contracts* significantly if the errors in BR($b \to s\gamma$) are added linearly, whereas there is little effect in the NUHM1.

This effect arises because the treatment of the BR($b \to s\gamma$) errors does not change the global χ^2 function at large $(m_0, m_{1/2})$, where its value approaches that of the "SM", since the experimental measurement of BR($b \to s\gamma$) is in good agreement with the SM prediction. On the other hand, adding the errors linearly relaxes the BR($b \to s\gamma$) constraint at smaller $(m_0, m_{1/2})$ in the CMSSM, reducing the tension with other observables and hence also the minimum of χ^2, as seen in Table 1. The net result is to enhance the rate of increase of χ^2 for CMSSM parameters departing from the best fit, implying that the 68% CL is reached more quickly. On the other hand, this effect is absent in the NUHM1 because the freedom to adjust the degree of Higgs non-universality already mitigates the tension of BR($b \to s\gamma$) with the other observables, leading to the 'pit' in the global χ^2 function mentioned above.

The $(\tan\beta, m_{1/2})$ *planes in the CMSSM and NUHM1*

Fig. 7 displays the $(\tan\beta, m_{1/2})$ planes in the CMSSM and NUHM1, exhibiting clearly the movement of the best-fit points and 68% and 95% CL contours to larger $\tan\beta$ that is driven by the tension between $(g-2)_\mu$ and the LHC push to larger $m_{1/2}$. Comparing the dotted and solid contours, we see that the LHC $\not{E}_T$ constraints force the new best-fit points into what were previously the 'tails' of the 95% CL regions at large $m_{1/2}$ and hence $\tan\beta$. However, it is clear that the range of $\tan\beta$ allowed at the 68% CL is still very broad, extending from < 20 to > 50 in both the CMSSM and the NUHM1. On the other hand, any future substantial increase in the LHC lower limit on $m_{1/2}$ would push $\tan\beta$ in both models into a narrower range ~ 50, where it encounters pressure from BR($B_s \to \mu^+\mu^-$) as discussed below.

The $(M_A, \tan\beta)$ *planes in the CMSSM and NUHM1*

We now turn to the $(M_A, \tan\beta)$ planes of the CMSSM and NUHM1, shown in Fig. 8, which are affected directly by the new CMS constraints on the heavy MSSM Higgs bosons $H/A, H^\pm$ [19, 21, 40], and by the CMS [22] and LHCb [23] constraints on BR($B_s \to \mu^+\mu^-$). As already discussed, we include the heavy Higgs constraints via the most sensitive CMS search for $H/A \to \tau^+\tau^-$ [21]. In evaluating the constraint on the $(M_A, \tan\beta)$ planes of the CMSSM and NUHM1 imposed by the new measurements of BR($B_s \to \mu^+\mu^-$), we use the official combination of the recent upper limits on BR($B_s \to \mu^+\mu^-$) from the CMS and LHCb Collaborations [41], which yields BR($B_s \to \mu^+\mu^-$) $< 1.08 \times 10^{-8}$ at the 95% CL. Our implementation actually includes the full likelihood function arising from this combination. The measurement of BR($B_s \to \mu^+\mu^-$) by the CDF Collaboration [24] is in some tension with the CMS/LHCb combination, but only at the $\Delta\chi^2 \sim 1$ level. However, since there is so far no official combination of the CDF result with those of CMS and LHCb, we limit ourselves to discussing later its compatibility with the predictions for BR($B_s \to \mu^+\mu^-$) of our global fits. We see in Fig. 8 that the general effect of the $\mathrm{LHC}_{1/\mathrm{fb}}$ data is to push the preferred range of M_A to larger values, as well as pushing $\tan\beta$ towards larger values.

The impacts of the H/A and BR($B_s \to \mu^+\mu^-$) constraints are less important in the CMSSM than in the NUHM1, so we discuss the latter in more detail. Fig. 9 shows four versions of the $(M_A, \tan\beta)$ plane in the NUHM1, with all the $\mathrm{LHC}_{1/\mathrm{fb}}$ constraints applied (upper left, equivalent to the right panel of Fig. 8), dropping the H/A constraint but keeping BR($B_s \to \mu^+\mu^-$) (upper right), dropping BR($B_s \to \mu^+\mu^-$) but keeping the H/A constraint (lower left), and dropping both constraints (lower right). Comparing the two upper panels, we see that the H/A

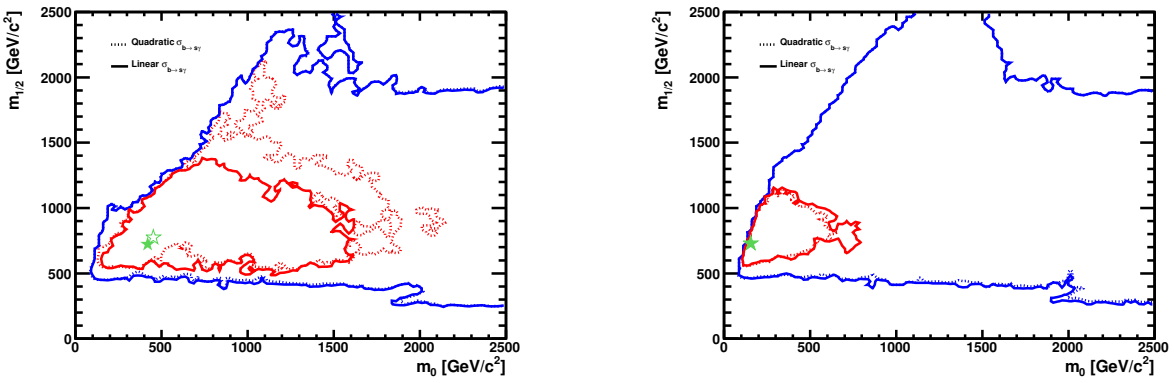

Figure 6. *The $(m_0, m_{1/2})$ planes in the CMSSM (left) and the NUHM1 (right). Here we show as solid lines the 68% and 95% CL contours obtained by adding linearly the experimental and theoretical errors in BR($b \to s\gamma$). The contours obtained by combining them quadratically as in Fig. 1 are shown here for comparison as dotted lines.*

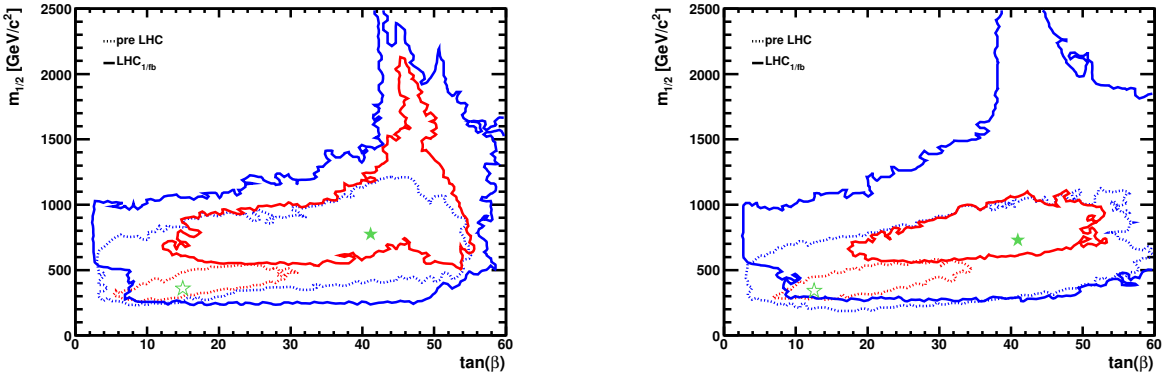

Figure 7. *The $(\tan\beta, m_{1/2})$ planes in the CMSSM (left) and the NUHM1 (right). In each plane, the best-fit point after incorporation of the LHC$_{1/\mathrm{fb}}$ constraints is indicated by a filled green star, and the pre-LHC fit [5] by an open star. The $\Delta\chi^2 = 2.30$ and 5.99 contours, commonly interpreted as the boundaries of the 68% and 95% CL regions, are indicated in red and blue, respectively, the solid lines including the LHC$_{1/\mathrm{fb}}$ data and the dotted lines showing the pre-LHC fits.*

constraint is relevant for $M_A \lesssim 450$ GeV, and that applying it impacts the low-M_A sides of the 68% and 95% CL contours, whereas the best-fit point is unaffected. Comparing the upper and lower panels, we see that the BR($B_s \to \mu^+\mu^-$) constraint is relevant for low M_A values. In particular, the 68% CL contours extend to slightly lower $\tan\beta$ values and the best-fit points (green stars) move to significantly lower $\tan\beta$ when BR($B_s \to \mu^+\mu^-$) is included. as seen in Fig. 9. Both the H/A and BR($B_s \to \mu^+\mu^-$) constraints have the potential for more significant impacts in

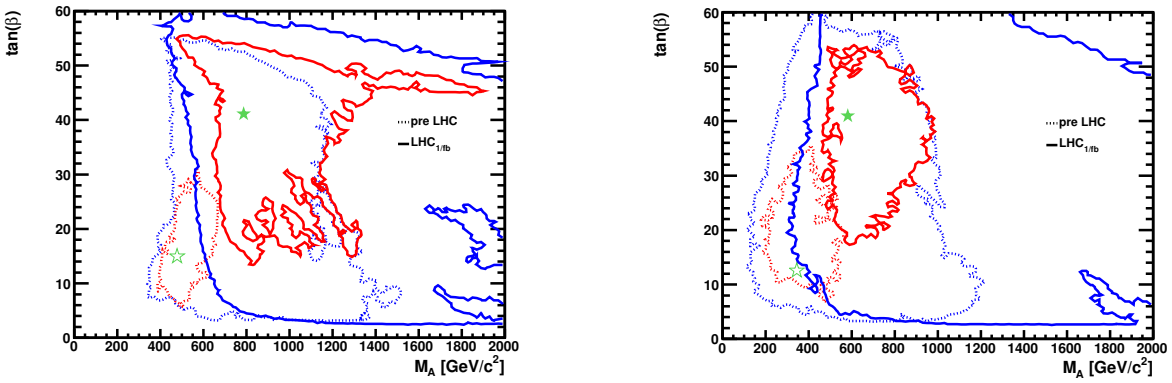

Figure 8. *The $(M_A, \tan\beta)$ planes in the CMSSM (left) and the NUHM1 (right). In each plane, the best-fit point after incorporation of the LHC$_{1/\mathrm{fb}}$ constraints is indicated by a filled green star, and the pre-LHC fit [5] by an open star. The $\Delta\chi^2 = 2.30$ and 5.99 contours, commonly interpreted as the boundaries of the 68 and 95% CL regions, are indicated in red and blue, respectively, the solid lines including the LHC$_{1/\mathrm{fb}}$ data and the dotted lines showing the pre-LHC fits.*

the future.

Predictions for $m_{\tilde{g}}$

In Fig. 10 we show the one-dimensional χ^2 functions predicted by global fits for $m_{\tilde{g}}$ in the CMSSM (left) and the NUHM1 (right). The solid lines are based on our global fits including the LHC$_{1/\mathrm{fb}}$ constraints, whereas the dotted lines are based on our previous global fits based on the pre-LHC constraints [5] [13]. We see that the best-fit estimates of $m_{\tilde{g}}$ have increased substantially to ~ 1600 GeV as a result of the LHC$_{1/\mathrm{fb}}$ data, but we also see that there is considerable uncertainty in this estimate, with $m_{\tilde{g}} > 2500$ GeV subject to a penalty $\Delta\chi^2 \sim 2$ only.

[13] The 'stalactites' at $m_{\tilde{g}} \sim 400$ GeV in the pre-LHC fits [5] were due to the light-Higgs funnel that has now been excluded by the LHC$_{1/\mathrm{fb}}$ data. Likewise, the 'stalactite' in the CMSSM LHC$_{1/\mathrm{fb}}$ curve also originates in the light-Higgs funnel region, and comes from points with large $m_0 > 3$ TeV - which is why they are not seen in Fig. 1 - and large A_0. These points might be excluded by the ATLAS 1/fb 0-lepton search, whose published $(m_0, m_{1/2})$ exclusion for $\tan\beta = 10$ and $A_0 = 0$ extends only to $m_0 = 3$ TeV.

Predictions for BR$(B_s \to \mu^+\mu^-)$

In Fig. 11 we show the one-dimensional χ^2 functions predicted by our global fits for BR$(B_s \to \mu^+\mu^-)$ in the CMSSM (left) and the NUHM1 (right). The solid lines are based on the official combination of the CMS and LHCb constraints on this decay [41], whereas the dashed lines show results using an unofficial combination of these constraints with the CDF measurement [24], and the dotted lines represent pre-LHC predictions [5]. We see that the best-fit estimates of BR$(B_s \to \mu^+\mu^-)$ are somewhat above the SM value, as a result of the push towards larger $\tan\beta$ required to accommodate the LHC data while reconciling them with $(g-2)_\mu$. In both the CMSSM and the NUHM1, the estimates of BR$(B_s \to \mu^+\mu^-)$ are quite compatible with an unofficial combined fit to CDF, CMS and LHCb data, where the main effect is a reduction of χ^2 in a somewhat broader range of BR$(B_s \to \mu^+\mu^-)$.

Predictions for M_h

In Fig. 12 we show the one-dimensional χ^2 functions predicted by our global fits for M_h in the CMSSM (left) and the NUHM1 (right). In this figure we *do not* include the direct limits from

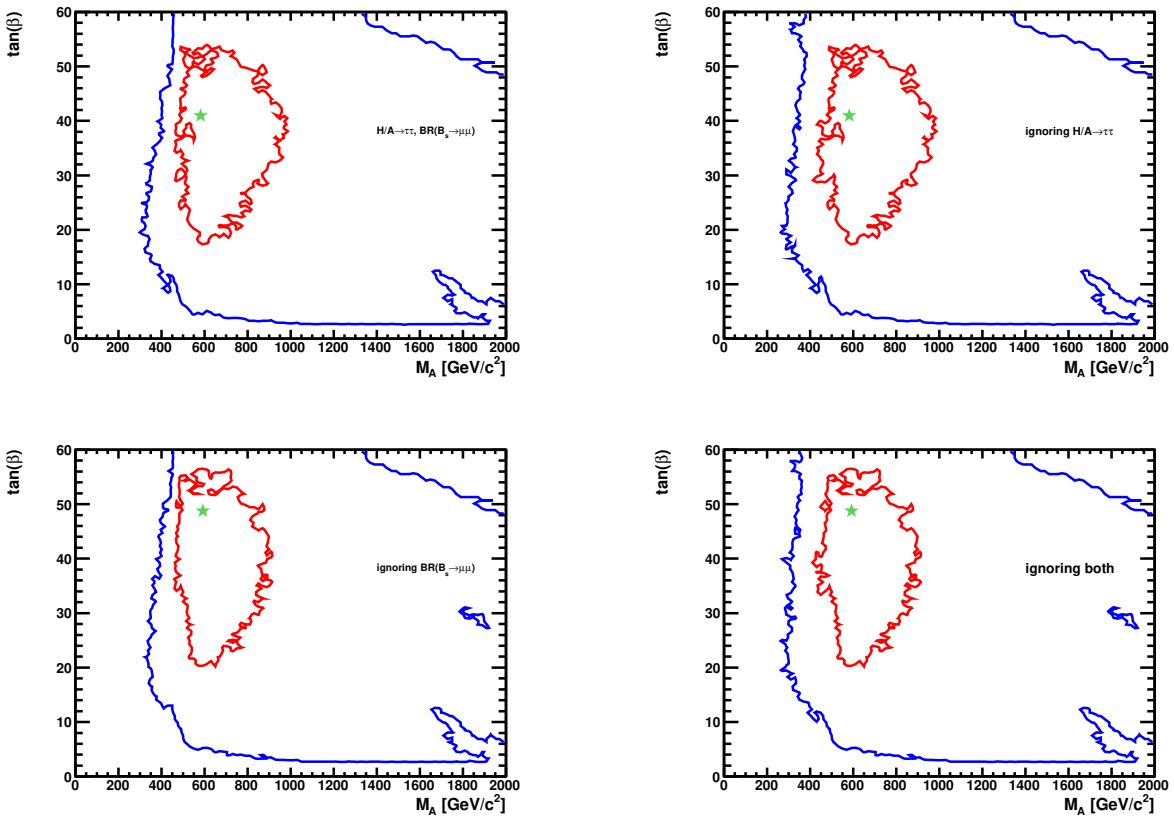

Figure 9. *The* $(M_A, \tan\beta)$ *planes in the NUHM1 including both the H/A [21] and* $\mathrm{BR}(B_s \to \mu^+\mu^-)$ *[41] constraints (upper left), dropping the H/A constraint but keeping the* $\mathrm{BR}(B_s \to \mu^+\mu^-)$ *constraint (upper right), dropping* $\mathrm{BR}(B_s \to \mu^+\mu^-)$ *but keeping H/A (lower left), and dropping both constraints (lower right).*

LEP [55, 56] or the Tevatron, so as to illustrate whether there is a conflict between these limits and the predictions of supersymmetric models. For each model we display the new likelihood functions corresponding to the $\mathrm{LHC}_{1/\mathrm{fb}}$ data set, indicating the theoretical uncertainty in the calculation of M_h of ~ 1.5 GeV by red bands. We also show, as dashed lines without red bands, our previous predictions based on the pre-LHC results (also discarding the LEP constraint). We see that the LHC data improve the consistency of the model predictions with the LEP exclusion, removing whatever tension existed previously. We cannot resist pointing out that the best-fit value for M_h found recently in a SM fit including LEP, Tevatron and LHC exclusions as well as precision electroweak data ~ 120 GeV [59], and that this is also the value of the SM Higgs mass that is most compatible with the ongoing LHC searches [63].

Predictions for M_A

In Fig. 13 we show the one-dimensional χ^2 functions predicted by our global fits for M_A in the CMSSM (left) and the NUHM1 (right). We see that the best-fit values of M_A have increased in both models, by ~ 350 GeV and ~ 250 GeV, respectively.

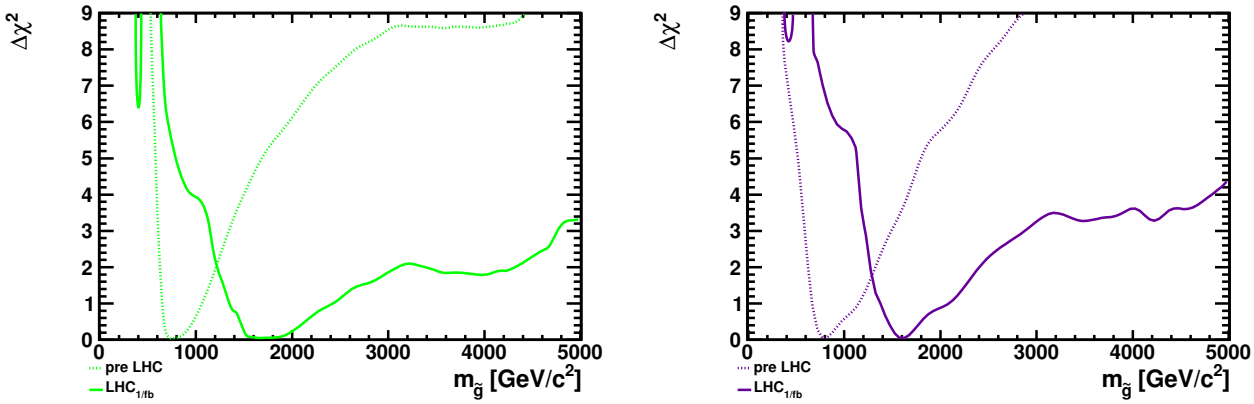

Figure 10. *The one-dimensional χ^2 functions for $m_{\tilde{g}}$ in the CMSSM (left) and the NUHM1 (right). The solid lines are for fits including the LHC$_{1/\rm fb}$ data, and the dotted lines are for fits based on the pre-LHC data [8].*

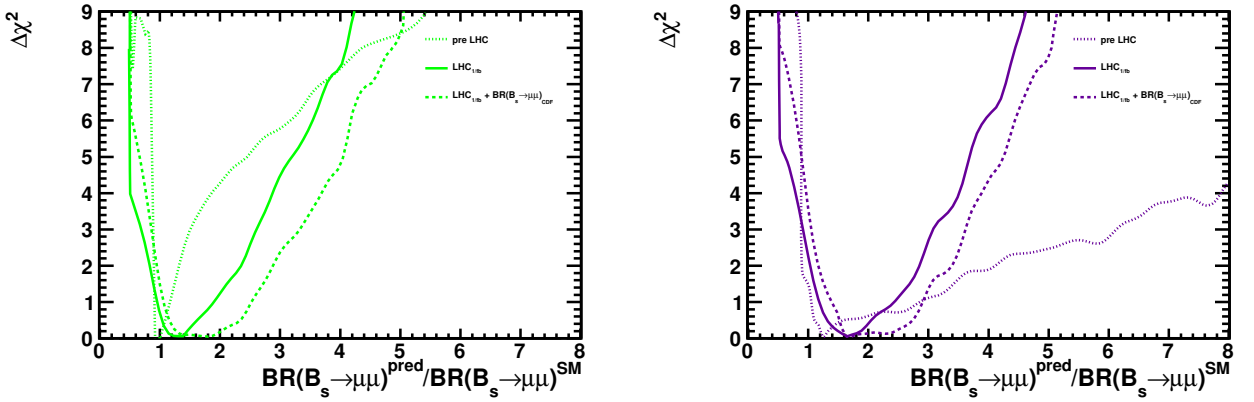

Figure 11. *The one-dimensional χ^2 functions for* BR$(B_s \to \mu^+\mu^-)$ *in the CMSSM (left) and the NUHM1 (right). The solid lines are for fits including the official combination of the results from the CMS and LHCb Collaborations [41], the dashed lines are for fits using an unofficial combination of these results with the CDF result [24], and the dotted lines represent pre-LHC predictions [5].*

Dark matter scattering cross sections

In Fig. 14 we show the 68% and 95% CL contours in the $(m_{\tilde{\chi}_1^0}, \sigma_p^{\rm SI})$ planes for the CMSSM (left) and the NUHM1 (right). The solid lines are based on our global fits including the LHC$_{1/\rm fb}$ constraints, whereas the dotted lines correspond to our previous fits using the pre-LHC constraints. In both cases, we assume $\Sigma_{\pi N} = 50 \pm 14$ MeV [35] [14], and we include with the LHC$_{1/\rm fb}$ data the XENON100 constraint on $\sigma_p^{\rm SI}$ [25]. We see that the LHC$_{1/\rm fb}$ data tend to push $m_{\tilde{\chi}_1^0}$ to larger values [15], and that these are correlated

[14] We recall the sensitivity of predictions for $\sigma_p^{\rm SI}$ to the uncertainty in $\Sigma_{\pi N}$ [8].

[15] The slivers of points at $m_{\tilde{\chi}_1^0} \sim 60$ GeV originate in the light-Higgs funnel region with large $m_0 > 3$ TeV men-

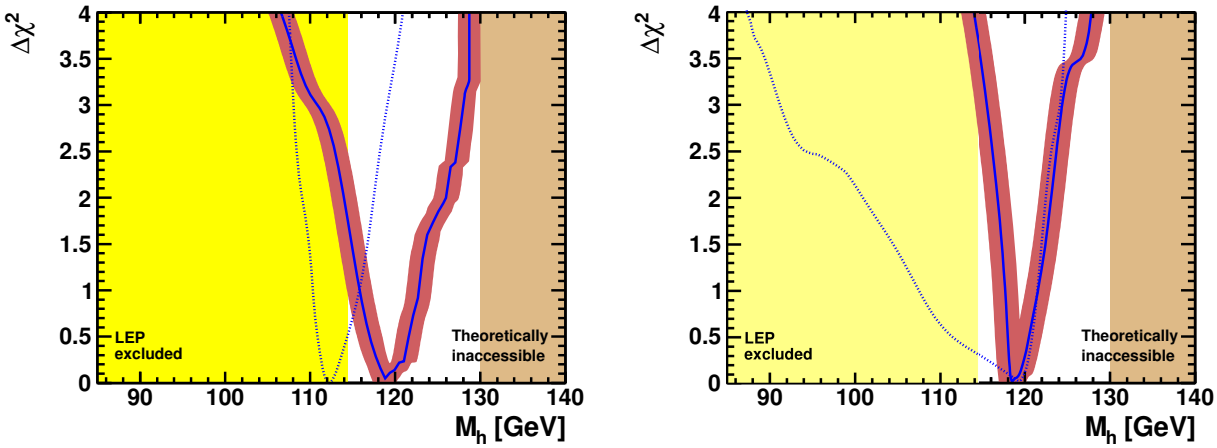

Figure 12. *The one-dimensional χ^2 functions for M_h in the CMSSM (left) and the NUHM1 (right). The solid lines are for fits including all the available data, except the LEP [55, 56] constraints, with a red band indicating the estimated theoretical uncertainty in the calculation of M_h of ~ 1.5 GeV. The pre-LHC results [5] are shown as dotted lines. The yellow shading in the left panel shows the LEP exclusion of an SM Higgs boson, which applies also to the lightest CMSSM Higgs boson [57, 58]. The lighter yellow shading in the right panel reflects the fact that this mass range is not completely excluded in the NUHM1 due to a possible suppression of the ZZh coupling. The beige shading in both panels indicates values of M_h inaccessible in the supersymmetric models studied with GUT-scale unification.*

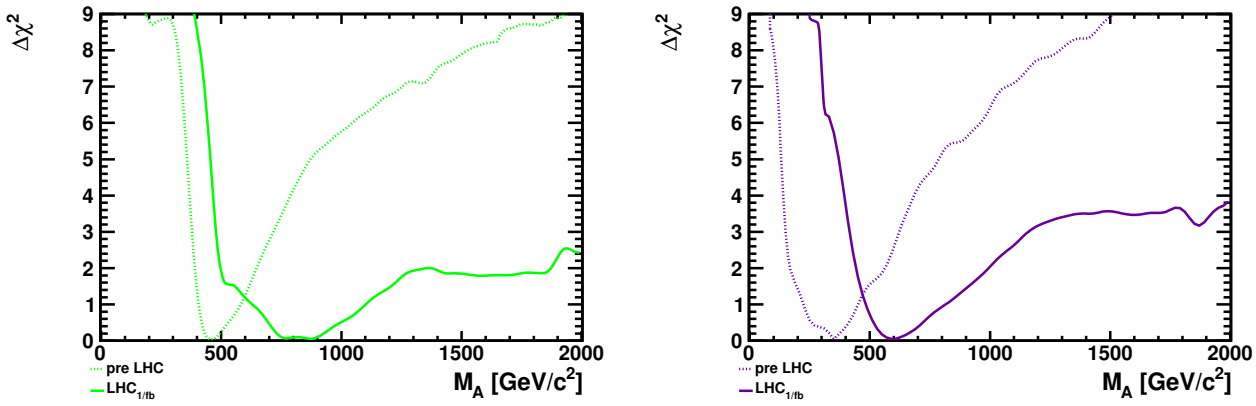

Figure 13. *The one-dimensional χ^2 functions for M_A in the CMSSM (left) and the NUHM1 (right). The solid lines are for fits including the $LHC_{1/\mathrm{fb}}$ data, and the dotted lines are for fits based on the pre-LHC data [5].*

tioned earlier, which might be excluded by the ATLAS 1/fb 0-lepton search.

with lower values of σ_p^{SI}, though with best-fit values still $\sim 10^{-45}$ cm^2. We do not present here pre-

dictions for spin-dependent scattering or signatures of astrophysical dark matter annihilations, which are further removed from the prospective experimental sensitivities in the near future.

Sparticle thresholds in e^+e^- annihilation

In view of the interest in building an e^+e^- collider as the next major project at the energy frontier, we now analyze the implications of the $\mathrm{LHC}_{1/\mathrm{fb}}$ and XENON100 data for expectations for sparticle production in e^+e^- annihilation within the CMSSM and NUHM1. In this respect it has to be kept in mind that the LHC searches are mainly sensitive to the production of coloured particles, whereas lepton colliders will have a high sensitivity in particular for the production of colour-neutral states, such as sleptons, charginos and neutralinos, as well as yielding high-precision measurements that will provide indirect sensitivity to quantum effects of new states. Anything inferred from the coloured sector concerning the uncoloured sector depends on the underlying model assumptions, and in particular on assumptions about the possible universality of soft supersymmetry breaking at the GUT scale. Non-universal models, e.g., low-energy supersymmetric models, or models with different GUT assumptions, could present very different possibilities.

Fig. 15 compares the likelihood functions for various thresholds in the CMSSM (upper panel) and the NUHM1 (lower panel), based on the global fits made using the $\mathrm{LHC}_{1/\mathrm{fb}}$ and XENON100 constraints. The lowest thresholds are those for $e^+e^- \to \tilde{\chi}_1^0\tilde{\chi}_1^0$, $\overline{\tilde{\tau}_1}\tilde{\tau}_1$, $\overline{\tilde{e}_R}\tilde{e}_R$ and $\overline{\tilde{\mu}_R}\tilde{\mu}_R$ (the latter is not shown, it is similar to that for $\overline{\tilde{e}_R}\tilde{e}_R$). We see that, within the CMSSM and NUHM1, it now seems that these thresholds may well lie above 500 GeV, though in the CMSSM significant fractions of their likelihood functions still lie below 500 GeV. The thresholds for $\tilde{\chi}_1^0\tilde{\chi}_2^0$ and $\overline{\tilde{e}_R}\tilde{e}_L + \overline{\tilde{e}_L}\tilde{e}_R$ are expected to be somewhat higher, possibly a bit below 1 TeV. The preferred value for the threshold for $\tilde{\chi}_1^\pm\tilde{\chi}_1^\mp$ lies at about 1700 GeV in both the CMSSM and NUHM1 scenarios, that for the HA threshold lies above 1 TeV, and that for first- and second-generation squark-antisquark pair production lies beyond 2.5 TeV in both models. It should be kept in mind that these high thresholds are linked with the reduced p-value of the model. Further increases in the excluded regions would yield even higher thresholds, but would also make the CMSSM or NUHM1 seem even less likely.

4. Summary and Conclusions

There is some disappointment in the air that the LHC has found no signs of supersymmetry in its first $\sim 1/\mathrm{fb}$ of data. However, it should be kept in mind that the searches performed at the LHC so far have essentially only been able to set limits on the production of the gluino and the squarks of the first two generations, and the resulting limits depend sensitively on the mass assumed for the lightest supersymmetric particle [64]. On the other hand, the sensitivities of direct searches for stops and sbottoms and colour-neutral superpartners are very limited up to now. This situation will improve, as several times more data can be expected by the end of 2012, there is the prospect subsequently of an increase in the energy by a factor up to two, and the LHC is expected eventually to accumulate orders of magnitude more data.

The initial optimistic prospects for SUSY searches at the LHC were largely driven by two indications that the supersymmetric mass scale might not be very high: $(g-2)_\mu$ and the need for dark matter that should not be overdense. Neither of these indications has weakened recently. Indeed, the $(g-2)_\mu$ hint has even strengthened with the convergence of the previously discrepant SM calculations using low-energy e^+e^- and τ decay data [42, 65]. However, as we have discussed in this paper, significant tension is now emerging between the $(g-2)_\mu$ constraint and LHC data within the specific context of the CMSSM and NUHM1. *A priori*, in a general SUSY model there is not necessarily a tension between a heavy gluino and heavy squarks of the first two generations on the one hand, as favoured by the LHC limits, and light colour-neutral states on the other hand, as favoured by $(g-2)_\mu$.

The tension within the CMSSM and NUHM1 can be reduced to some extent by adopting a

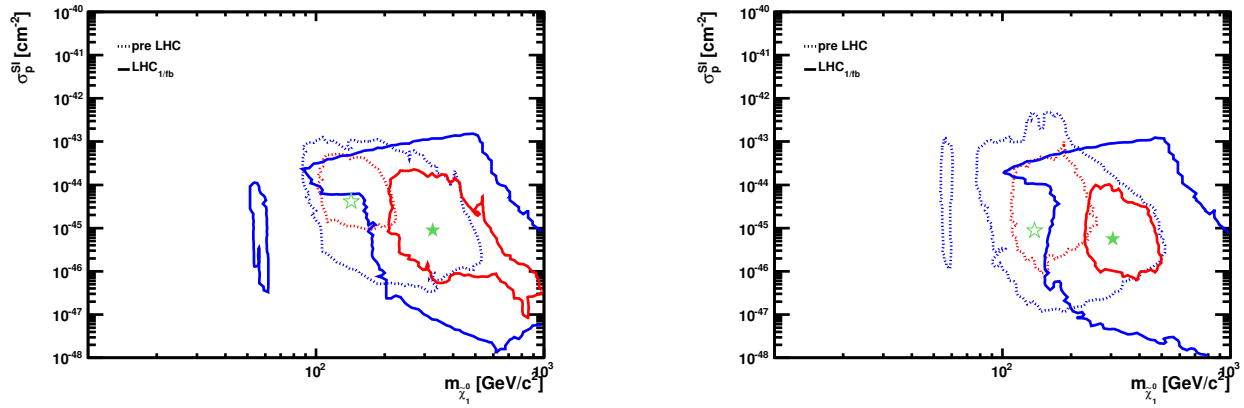

Figure 14. *The 68% and 95% CL contours (red and blue, respectively) in the CMSSM (left) and the NUHM1 (right). The solid lines are for fits including the XENON100 [25] and LHC*$_{1/\mathrm{fb}}$ *data, whereas the dotted lines include only the pre-LHC data [5].*

larger value of $\tan\beta$, but this may eventually lead to subsidiary tension with the LHC H/A constraints and the tightening experimental vise on BR($B_s \to \mu^+\mu^-$). In any case, it will be important to subject the $(g-2)_\mu$ constraint to closer scrutiny, and the upcoming Fermilab and J-PARC experiments on $(g-2)_\mu$ [66] are most welcome and timely in this regard. In parallel, refinements of the experimental inputs for the prediction of $(g-2)_\mu$ from both low-energy e^+e^- and τ decay data would also be welcome. It will be also necessary to subject the theoretical calculations within the SM and the corresponding estimates of the remaining theoretical uncertainties to further scrutiny.

The dark matter upper limit on the sparticle mass scale remains unchanged, and is responsible for the disfavoured region above $m_{1/2} \sim$ 2500 GeV visible in our figures for the CMSSM and the NUHM1. On the other hand, the dark matter constraint on m_0 is not so strong, as also seen in the figures, extending well beyond the range displayed. Considering the impact of direct jets $+\not{E}_T$ searches only, the regions of the CMSSM and NUHM1 $(m_0, m_{1/2})$ planes in Fig. 2 with p-values significantly non-zero extend beyond the likely reach even of the full-energy LHC in its high-luminosity incarnation. *A fortiori*, the same is true for the regions of these planes allowed at the current 95% CL ($\Delta\chi^2 = 5.99$ relative to the global minima, bounded by the blue contours in Fig. 1). This is even more true of the full regions of the CMSSM and NUHM1 $(m_0, m_{1/2})$ planes that are allowed by the dark matter constraint.

In light of this discussion, under what circumstances could one conclude that the CMSSM or NUHM1 is excluded? Currently, our best fits in both these models have p-values above 10%, comparable to that of SM fits to precision electroweak data from LEP and SLD, and the F-test shows that both the CMSSM and NUHM1 are warranted extensions of the SM, in the sense that introducing their parameters provides an improvement in χ^2 that is valuable in both cases. Moreover, it seems unlikely that the LHC will soon be able to explore all the region of the $(m_0, m_{1/2})$ planes in Fig. 2 where the models' p-values exceed 5%, nor does the LHC seem likely soon to push F_χ (see Fig. 3) to uninterestingly low levels. This is not surprising, as in the high-mass limit the superpartners decouple and one is left essentially with the SM with a light Higgs.

One way for the LHC to invalidate the models studied here would be to discover an SM-like

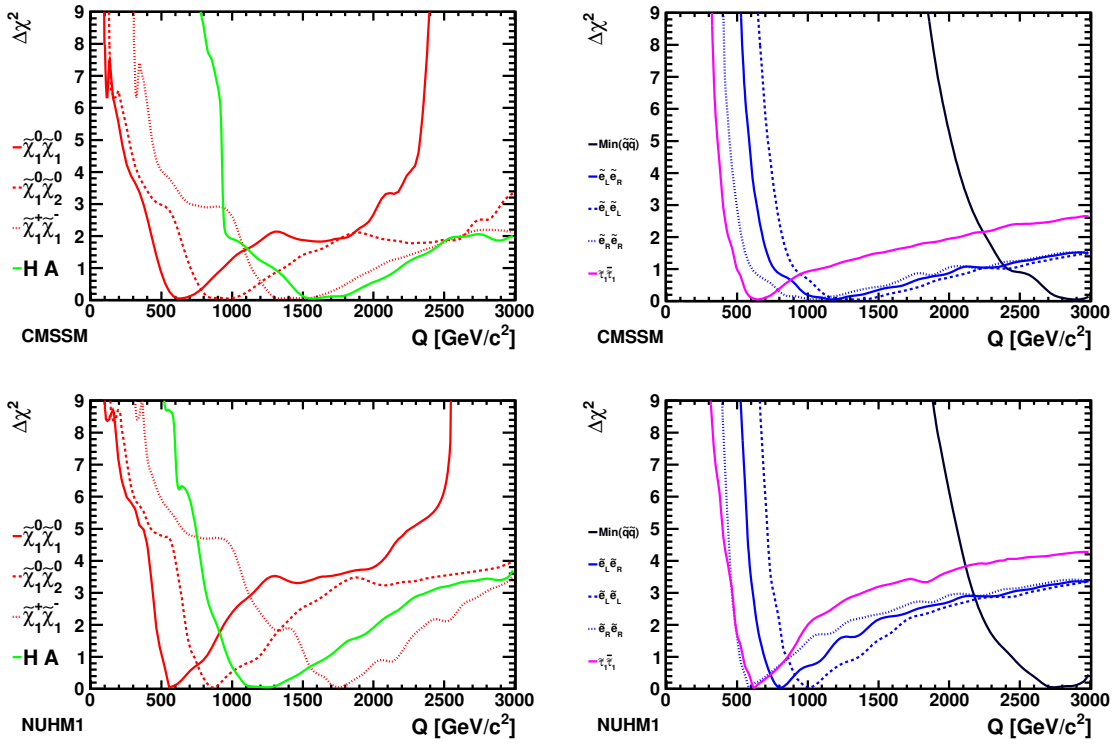

Figure 15. *The χ^2 likelihood functions for various pair-production thresholds in e^+e^-, as estimated in the CMSSM (upper panel) and the NUHM1 (lower panel) after incorporating the XENON100 [25] and LHC$_{1/\mathrm{fb}}$ constraints. The likelihood function for the $\widetilde{\mu}_R\tilde{\mu}_R$ threshold (not shown) is very similar to that for $\widetilde{e}_R\tilde{e}_R$.*

Higgs boson weighing substantially more than the range ~ 120 GeV predicted in Fig 12. A value of $M_h \sim 125$ GeV or more would be in some tension with $(g-2)_\mu$, and perhaps hint towards models beyond the CMSSM and NUHM1, whereas a value of ~ 130 GeV or more would cast severe doubt on most simple GUT-based models. As already mentioned, range $M_h \sim 120$ to 130 GeV is precisely that currently favoured independently by precision electroweak data and by LEP, Tevatron and LHC searches. If a Higgs-like signal were to be discovered in the lower part of this range, supersymmetry might not be far away, whereas if M_h is in the upper part of this range, indicating that at least the third-generation squarks could be heavy, one might for some time be in the frustrating situation of acquiring ever more circumstantial hints for supersymmetry, but with no direct evidence. On the other hand, if the LHC discovers that $M_h > 130$ GeV, the time might come to take another look at non-minimal supersymmetric models.

Acknowledgements

The work of O.B., J.E. and K.A.O. is supported partly by the London Centre for Terauniverse Studies (LCTS), using funding from the European Research Council via the Advanced Investigator Grant 267352. The work of S.H. was supported in part by CICYT (grant FPA 2010–22163-C02-01) and by the Spanish MICINN's Consolider-Ingenio 2010 Program under grant MultiDark CSD2009-00064. The work of K.A.O. is supported in part by DOE grant DE-FG02-94ER-40823 at the University of Minnesota.

REFERENCES

1. O. Buchmueller *et al.*, Phys. Lett. B **657** (2007) 87 [arXiv:0707.3447 [hep-ph]].
2. O. Buchmueller *et al.*, JHEP **0809** (2008) 117 [arXiv:0808.4128 [hep-ph]].
3. O. Buchmueller *et al.*, Eur. Phys. J. C **64** (2009) 391 [arXiv:0907.5568 [hep-ph]].
4. O. Buchmueller *et al.*, Phys. Rev. D **81** (2010) 035009 [arXiv:0912.1036 [hep-ph]].
5. O. Buchmueller *et al.*, Eur. Phys. J. C **71** (2011) 1583 [arXiv:1011.6118 [hep-ph]].
6. For a sampling of other pre-LHC analyses, see: E. A. Baltz and P. Gondolo, JHEP **0410** (2004) 052 [arXiv:hep-ph/0407039]; B. C. Allanach and C. G. Lester, Phys. Rev. D **73** (2006) 015013 [arXiv:hep-ph/0507283]; R. R. de Austri, R. Trotta and L. Roszkowski, JHEP **0605** (2006) 002 [arXiv:hep-ph/0602028]; R. Lafaye, T. Plehn, M. Rauch and D. Zerwas, Eur. Phys. J. C **54** (2008) 617 [arXiv:0709.3985 [hep-ph]]; S. Heinemeyer, X. Miao, S. Su and G. Weiglein, JHEP **0808** (2008) 087 [arXiv:0805.2359 [hep-ph]]; R. Trotta, F. Feroz, M. P. Hobson, L. Roszkowski and R. Ruiz de Austri, JHEP **0812** (2008) 024 [arXiv:0809.3792 [hep-ph]]; P. Bechtle, K. Desch, M. Uhlenbrock and P. Wienemann, Eur. Phys. J. C **66** (2010) 215 [arXiv:0907.2589 [hep-ph]].
7. O. Buchmueller *et al.*, Eur. Phys. J. C **71** (2011) 1634 [arXiv:1102.4585 [hep-ph]].
8. O. Buchmueller *et al.*, Eur. Phys. J. C **71** (2011) 1722 [arXiv:1106.2529 [hep-ph]].
9. For more information and updates, please see `http://cern.ch/mastercode/`.
10. D. Feldman, K. Freese, P. Nath, B. D. Nelson and G. Peim, arXiv:1102.2548 [hep-ph]; B. C. Allanach, arXiv:1102.3149 [hep-ph]; S. Scopel, S. Choi, N. Fornengo and A. Bottino, arXiv:1102.4033 [hep-ph]; P. Bechtle *et al.*, arXiv:1102.4693 [hep-ph]; B. C. Allanach, T. J. Khoo, C. G. Lester and S. L. Williams, arXiv:1103.0969 [hep-ph]; S. Akula, N. Chen, D. Feldman, M. Liu, Z. Liu, P. Nath and G. Peim, arXiv:1103.1197 [hep-ph]; M. J. Dolan, D. Grellscheid, J. Jaeckel, V. V. Khoze and P. Richardson, arXiv:1104.0585 [hep-ph]; S. Akula, D. Feldman, Z. Liu, P. Nath and G. Peim, arXiv:1103.5061 [hep-ph] (v2); M. Farina, M. Kadastik, D. Pappadopulo, J. Pata, M. Raidal and A. Strumia, arXiv:1104.3572 [hep-ph]; S. Profumo, arXiv:1105.5162 [hep-ph]; T. Li, J. A. Maxin, D. V. Nanopoulos and J. W. Walker, arXiv:1106.1165 [hep-ph].
11. H. P. Nilles, Phys. Rep. **110** (1984) 1; H. E. Haber and G. L. Kane, Phys. Rept. **117** (1985) 75.
12. H. Goldberg, Phys. Rev. Lett. **50** (1983) 1419; J. Ellis, J. Hagelin, D. Nanopoulos, K. Olive and M. Srednicki, Nucl. Phys. B **238** (1984) 453.
13. E. Komatsu *et al.* [WMAP Collaboration], Astrophys. J. Suppl. **192** (2011) 18 [arXiv:1001.4538 [astro-ph.CO]]; `http://lambda.gsfc.nasa.gov/product/map/current/parameters.cfm`.
14. M. Drees and M. M. Nojiri, Phys. Rev. D **47** (1993) 376 [arXiv:hep-ph/9207234]; G. L. Kane, C. F. Kolda, L. Roszkowski and J. D. Wells, Phys. Rev. D **49** (1994) 6173 [arXiv:hep-ph/9312272]; H. Baer and M. Brhlik, Phys. Rev. D **53** (1996) 597 [arXiv:hep-ph/9508321]; Phys. Rev. D **57** (1998) 567 [arXiv:hep-ph/9706509]; J. R. Ellis, T. Falk, K. A. Olive and M. Schmitt, Phys. Lett. B **388** (1996) 97 [arXiv:hep-ph/9607292]; Phys. Lett. B **413** (1997) 355 [arXiv:hep-ph/9705444]; J. R. Ellis, T. Falk, G. Ganis, K. A. Olive and M. Schmitt, Phys. Rev. D **58** (1998)

095002 [arXiv:hep-ph/9801445]; V. D. Barger and C. Kao, Phys. Rev. D **57** (1998) 3131 [arXiv:hep-ph/9704403]; J. R. Ellis, T. Falk, G. Ganis and K. A. Olive, Phys. Rev. D **62** (2000) 075010 [arXiv:hep-ph/0004169]; J. R. Ellis, T. Falk, G. Ganis, K. A. Olive and M. Srednicki, Phys. Lett. B **510** (2001) 236 [arXiv:hep-ph/0102098]; V. D. Barger and C. Kao, Phys. Lett. B **518** (2001) 117 [arXiv:hep-ph/0106189]; L. Roszkowski, R. Ruiz de Austri and T. Nihei, JHEP **0108** (2001) 024 [arXiv:hep-ph/0106334]; A. Djouadi, M. Drees and J. L. Kneur, JHEP **0108** (2001) 055 [arXiv:hep-ph/0107316]; U. Chattopadhyay, A. Corsetti and P. Nath, Phys. Rev. D **66** (2002) 035003 [arXiv:hep-ph/0201001]; J. R. Ellis, K. A. Olive and Y. Santoso, New Jour. Phys. **4** (2002) 32 [arXiv:hep-ph/0202110]; H. Baer, C. Balazs, A. Belyaev, J. K. Mizukoshi, X. Tata and Y. Wang, JHEP **0207** (2002) 050 [arXiv:hep-ph/0205325]; R. Arnowitt and B. Dutta, arXiv:hep-ph/0211417.

15. H. Baer, A. Mustafayev, S. Profumo, A. Belyaev and X. Tata, Phys. Rev. D **71** (2005) 095008 [arXiv:hep-ph/0412059]; H. Baer, A. Mustafayev, S. Profumo, A. Belyaev and X. Tata, *JHEP* **0507** (2005) 065, hep-ph/0504001; J. R. Ellis, K. A. Olive and P. Sandick, Phys. Rev. D **78** (2008) 075012 [arXiv:0805.2343 [hep-ph]].
16. J. R. Ellis, K. A. Olive, Y. Santoso and V. C. Spanos, Phys. Lett. B **573** (2003) 162 [arXiv:hep-ph/0305212], and Phys. Rev. D **70** (2004) 055005 [arXiv:hep-ph/0405110].
17. J. Polonyi, *Generalization Of The Massive Scalar Multiplet Coupling To The Supergravity,* Hungary Central Inst Res - KFKI-77-93; E. Cremmer, B. Julia, J. Scherk, P. van Nieuwenhuizen, S. Ferrara and L. Girardello, Phys. Lett. B **79**, 231 (1978); E. Cremmer, B. Julia, J. Scherk, S. Ferrara, L. Girardello and P. van Nieuwenhuizen, Nucl. Phys. B **147**, 105 (1979); R. Barbieri, S. Ferrara and C. A. Savoy, Phys. Lett. B **119**, 343 (1982); A. H. Chamseddine, R. L. Arnowitt and P. Nath, Phys. Rev. Lett. **49**, 970 (1982).
18. G. Aad *et al.* [ATLAS Collaboration], arXiv:1109.6572 [hep-ex].
19. ATLAS Collaboration, `https://atlas.web.cern.ch/Atlas/GROUPS/PHYSICS/CONFNOTES/ATLAS-CONF-2011-132/ATLAS-CONF-2011-132.pdf`.
20. S. Chatrchyan *et al.* [CMS Collaboration], arXiv:1109.2352 [hep-ex].
21. CMS Collaboration, `http://cdsweb.cern.ch/record/1378096/files/HIG-11-020-pas.pdf`.
22. S. Chatrchyan *et al.* [CMS Collaboration], arXiv:1107.5834 [hep-ex].
23. R. Aaij *et al.* [LHCb Collaboration], Phys. Lett. B **699** (2011) 330 [arXiv:1103.2465 [hep-ex]].
24. T. Aaltonen *et al.* [CDF Collaboration], arXiv:1107.2304 [hep-ex].
25. E. Aprile *et al.* [XENON100 Collaboration], arXiv:1104.2549 [astro-ph.CO].
26. S. Heinemeyer *et al.*, JHEP **0608** (2006) 052 [arXiv:hep-ph/0604147]; S. Heinemeyer, W. Hollik, A. M. Weber and G. Weiglein, JHEP **0804** (2008) 039 [arXiv:0710.2972 [hep-ph]].
27. B. C. Allanach, Comput. Phys. Commun. **143** (2002) 305 [arXiv:hep-ph/0104145].
28. G. Degrassi, S. Heinemeyer, W. Hollik, P. Slavich and G. Weiglein, Eur. Phys. J. C **28** (2003) 133 [arXiv:hep-ph/0212020]; S. Heinemeyer, W. Hollik and G. Weiglein, Eur. Phys. J. C **9** (1999) 343 [arXiv:hep-ph/9812472]; S. Heinemeyer, W. Hollik and G. Weiglein, Comput. Phys. Commun. **124** (2000) 76 [arXiv:hep-ph/9812320]; M. Frank *et al.*, JHEP **0702** (2007) 047 [arXiv:hep-ph/0611326]; See `http://www.feynhiggs.de` .
29. G. Isidori and P. Paradisi, Phys. Lett. B **639** (2006) 499 [arXiv:hep-ph/0605012]; G. Isidori, F. Mescia, P. Paradisi and D. Temes, Phys. Rev. D **75** (2007) 115019 [arXiv:hep-ph/0703035], and references therein.
30. F. Mahmoudi, Comput. Phys. Commun. **178** (2008) 745 [arXiv:0710.2067 [hep-ph]]; Comput. Phys. Commun. **180** (2009) 1579 [arXiv:0808.3144 [hep-ph]]; D. Eriksson, F. Mahmoudi and O. Stal, JHEP **0811** (2008)

035 [arXiv:0808.3551 [hep-ph]].
31. G. Belanger, F. Boudjema, A. Pukhov and A. Semenov, Comput. Phys. Commun. **176** (2007) 367 [arXiv:hep-ph/0607059]; Comput. Phys. Commun. **149** (2002) 103 [arXiv:hep-ph/0112278]; Comput. Phys. Commun. **174** (2006) 577 [arXiv:hep-ph/0405253].
32. Information about this code is available from K. A. Olive: it contains important contributions from T. Falk, A. Ferstl, G. Ganis, A. Mustafayev, J. McDonald, K. A. Olive, P. Sandick, Y. Santoso and M. Srednicki.
33. P. Skands *et al.*, JHEP **0407** (2004) 036 [arXiv:hep-ph/0311123]; B. Allanach *et al.*, Comput. Phys. Commun. **180** (2009) 8 [arXiv:0801.0045 [hep-ph]].
34. B. Dutta, Y. Mimura and Y. Santoso, arXiv:1107.3020 [hep-ph]; S. Akula, D. Feldman, P. Nath and G. Peim, arXiv:1107.3535 [hep-ph]; A. G. Akeroyd, F. Mahmoudi and D. Martínez Santos, arXiv:1108.3018 [hep-ph].
35. A. Bottino, F. Donato, N. Fornengo and S. Scopel, Astropart. Phys. **13** (2000) 215 [arXiv:hep-ph/9909228]; E. Accomando, R. L. Arnowitt, B. Dutta and Y. Santoso, Nucl. Phys. B **585** (2000) 124 [arXiv:hep-ph/0001019]; J. R. Ellis, K. A. Olive, Y. Santoso and V. C. Spanos, Phys. Rev. D **71** (2005) 095007 [arXiv:hep-ph/0502001]; J. R. Ellis, K. A. Olive and C. Savage, Phys. Rev. D **77** (2008) 065026 [arXiv:0801.3656 [hep-ph]]; J. Gasser, H. Leutwyler and M. E. Sainio, Phys. Lett. B **253** (1991) 252; M. Knecht, PiN Newslett. **15** (1999) 108 [arXiv:hep-ph/9912443]; M. E. Sainio, PiN Newslett. **16** (2002) 138 [arXiv:hep-ph/0110413]; B. Borasoy and U. G. Meissner, Annals Phys. **254** (1997) 192 [arXiv:hep-ph/9607432]; M. M. Pavan, I. I. Strakovsky, R. L. Workman and R. A. Arndt, PiN Newslett. **16** (2002) 110 [arXiv:hep-ph/0111066]; see also T. Strauch *et al.*, arXiv:1011.2415 [nucl-ex], as interpreted in V. Baru, C. Hanhart, M. Hoferichter, B. Kubis, A. Nogga and D. R. Phillips, arXiv:1003.4444 [nucl-th].
36. ATLAS Collaboration, `http://cdsweb.cern.ch/record/1358623/files/ATLAS-CONF-2011-090.pdf`.
37. CMS Collaboration, `http://cdsweb.cern.ch/record/1370064/files/SUS-11-010-pas.pdf`; `http://cdsweb.cern.ch/record/1370065/files/SUS-11-011-pas.pdf`.
38. ATLAS Collaboration, `http://cdsweb.cern.ch/record/1369212/files/ATLAS-CONF-2011-098.pdf`.
39. ATLAS Collaboration, ATLAS-CONF-2011-130.
40. CMS Collaboration, `https://twiki.cern.ch/twiki/bin/view/CMSPublic/Hig11008TWiki`.
41. CMS and LHCb Collaborations, `http://cdsweb.cern.ch/record/1374913/files/BPH-11-019-pas.pdf`.
42. M. Davier, A. Hoecker, B. Malaescu and Z. Zhang, Eur. Phys. J. C **71** (2011) 1515 [arXiv:1010.4180 [hep-ph]].
43. CDF and D0 Collaborations, arXiv:1007.3178 [hep-ex].
44. ALEPH, CDF, D0, DELPHI, L3, OPAL, SLD Collaborations, the LEP Electroweak Working Group, the Tevatron Electroweak Working Group and the SLD electroweak and heavy flavour groups, arXiv:1012.2367 [hep-ex], as updated in July 2011 on `http://lepewwg.web.cern.ch/LEPEWWG/plots/summer2011/`.
45. M. Misiak *et al.*, Phys. Rev. Lett. **98** (2007) 022002 [arXiv:hep-ph/0609232]; M. Ciuchini, G. Degrassi, P. Gambino and G. F. Giudice, Nucl. Phys. B **534** (1998) 3 [arXiv:hep-ph/9806308]; G. Degrassi, P. Gambino and G. F. Giudice, JHEP **0012** (2000) 009 [arXiv:hep-ph/0009337]; M. S. Carena, D. Garcia, U. Nierste and C. E. M. Wagner, Phys. Lett. B **499** (2001) 141 [arXiv:hep-ph/0010003]; G. D'Ambrosio, G. F. Giudice, G. Isidori and A. Strumia, Nucl. Phys. B **645** (2002) 155 [arXiv:hep-ph/0207036].
46. The Heavy Flavor Averaging Group, D. Asner *et al.*, arXiv:1010.1589

[hep-ex], with updates available at http://www.slac.stanford.edu/xorg/hfag/osc/end_2009.
47. C. Bobeth, A. J. Buras and T. Ewerth, Nucl. Phys. B **713** (2005) 522 [arXiv:hep-ph/0409293].
48. M. Antonelli *et al.* [FlaviaNet Working Group on Kaon Decays], arXiv:0801.1817 [hep-ph].
49. A. J. Buras, P. Gambino, M. Gorbahn, S. Jager and L. Silvestrini, Nucl. Phys. B **592** (2001) 55 [arXiv:hep-ph/0007313].
50. A. V. Artamonov *et al.* [The E949 Collaboration], arXiv:0808.2459 [hep-ex].
51. M. Bona *et al.* [UTfit Collaboration], JHEP **0803** (2008) 049 [arXiv:0707.0636 [hep-ph]].
52. V. Lubicz and C. Tarantino, Nuovo Cim. B **123** (2008) 674 [arXiv:0807.4605 [hep-lat]].
53. D. Stockinger, J. Phys. G **34** (2007) R45 [arXiv:hep-ph/0609168]; J. Miller, E. de Rafael and B. Roberts, *Rept. Prog. Phys.* **70** (2007) 795 [arXiv:hep-ph/0703049]; J. Prades, E. de Rafael and A. Vainshtein, arXiv:0901.0306 [hep-ph]; F. Jegerlehner and A. Nyffeler, Phys. Rept. **477**, 1 (2009) [arXiv:0902.3360 [hep-ph]]; M. Davier, A. Hoecker, B. Malaescu, C. Z. Yuan and Z. Zhang, Eur. Phys. J. C **66**, 1 (2010) [arXiv:0908.4300 [hep-ph]]. J. Prades, Acta Phys. Polon. Supp. **3**, 75 (2010) [arXiv:0909.2546 [hep-ph]]; T. Teubner, K. Hagiwara, R. Liao, A. D. Martin and D. Nomura, arXiv:1001.5401 [hep-ph].
54. G. Bennett et al. [The Muon g-2 Collaboration], *Phys. Rev. Lett.* **92** (2004) 161802, [arXiv:hep-ex/0401008]; and *Phys. Rev.* **D 73** (2006) 072003 [arXiv:hep-ex/0602035].
55. R. Barate *et al.* [ALEPH, DELPHI, L3, OPAL Collaborations and LEP Working Group for Higgs boson searches], Phys. Lett. B **565** (2003) 61 [arXiv:hep-ex/0306033].
56. S. Schael *et al.* [ALEPH, DELPHI, L3, OPAL Collaborations and LEP Working Group for Higgs boson searches], Eur. Phys. J. C **47** (2006) 547 [arXiv:hep-ex/0602042].
57. J. R. Ellis, S. Heinemeyer, K. A. Olive and G. Weiglein, Phys. Lett. B **515** (2001) 348 [arXiv:hep-ph/0105061].
58. S. Ambrosanio, A. Dedes, S. Heinemeyer, S. Su and G. Weiglein, Nucl. Phys. B **624** (2002) 3 [arXiv:hep-ph/0106255].
59. M. Baak *et al.*, arXiv:1107.0975 [hep-ph].
60. J. R. Ellis, K. Enqvist, D. V. Nanopoulos and F. Zwirner, Mod. Phys. Lett. A **1** (1986) 57; R. Barbieri and G. F. Giudice, Nucl. Phys. B **306** (1988) 63.
61. C. Kim, A. K. Leibovich, T. Mehen, Phys. Rev. **D78** (2008) 054024. [arXiv:0805.1735 [hep-ph]].
62. T. Becher, R. J. Hill and M. Neubert, Phys. Rev. D **72** (2005) 094017 [arXiv:hep-ph/0503263].
63. ATLAS Collaboration, https://atlas.web.cern.ch/Atlas/GROUPS/PHYSICS/CONFNOTES/ATLAS-CONF-2011-135/ATLAS-CONF-2011-135.pdf; CMS Collaboration, http://cdsweb.cern.ch/record/1376643/files/HIG-11-022-pas.pdf.
64. T. J. LeCompte and S. P. Martin, arXiv:1105.4304 [hep-ph]; J. Fan, M. Reece and J. T. Ruderman, arXiv:1105.5135 [hep-ph].
65. F. Jegerlehner and R. Szafron, Eur. Phys. J. C **71** (2011) 1632 [arXiv:1101.2872 [hep-ph]].
66. R. M. Carey *et al.*, New g-2 Collaboration, http://gm2.fnal.gov/; For a summary of the J-PARC proposal, please see Y. Okada, https://indico.cern.ch/getFile.py/access?contribId=4&sessionId=1&resId=0&materialId=slides&confId=113370.